

BASELINE EROSION RATES FOR THE FERNAN WATERSHED INFERRED FROM
COSMOGENIC ^{10}Be CONCENTRATIONS: COMPARING EROSION AND SEDIMENT YIELDS
OVER DIFFERENT TIME-SCALES

A Thesis

Presented in Partial Fulfillment of the Requirements for the

Degree of Master of Science

with a

Major in Geological Sciences

in the

College of Graduate Studies

University of Idaho

by

Cody Parker

Major Professor: Brian Yanites, Ph.D.

Committee Members: William Phillips, Ph.D., Frank Wilhelm, Ph.D.

Department Administrator: Mickey Gunter, Ph.D.

August 2016

AUTHORIZATION TO SUBMIT

This thesis of Cody Parker, submitted for the degree of Master of Science with a Major in Geology and titled "Baseline Erosion Rates for the Fernan Watershed Inferred from Cosmogenic ^{10}Be Concentrations: Comparing Erosion and Sediment Yield Over Different Time Scales," has been reviewed in final form. Permission, as indicated by the signatures and dates below, is now granted to submit final copies to the College of Graduate Studies for approval.

Major Professor _____ Date _____
Brian J. Yanites Ph.D.

Committee
Members _____ Date _____
Frank M. Wilhelm Ph.D.

_____ Date _____
William M. Phillips Ph.D.

Department
Administrator _____ Date _____
Mickey Gunter Ph.D.

ABSTRACT

Since the 1990's, decreased water quality of Fernan Lake has raised concerns about the suitability of the water in the lake for domestic and recreational use. State regulatory agencies have suggested that changes in land use throughout the watershed have increased soil erosion rates, and thus sediment yield to the lake, above the baseline rate which may be contributing to the poor water quality. However, the baseline rate of erosion has not been explicitly addressed, and is the focus of this study. I constructed a long-term sediment budget for the upland watershed based on processes integrated over 8-20 ky to test the hypothesis that sediment delivery to the lake has not changed over time, and that changes in land use have not altered erosion rates. Cosmogenic ^{10}Be concentrations in alluvial sediment record erosion rates ranging from $\sim 0.031 \pm 0.002 \text{ mm yr}^{-1}$ to $\sim 0.067 \pm 0.011 \text{ mm yr}^{-1}$ for 6 sub-basins throughout the watershed. The ^{10}Be method integrates erosion rates over 8,000 to 20,000 year time-scales, averaging over short-term variability of erosion due to changes in land use and hydrologic factors. I compared these rates to sediment storage rates inferred from sediment cores taken from the floodplain (spanning $\sim 11,000$ years), to estimate the baseline rate of sediment delivery to the lake. Then, I compared the baseline sediment yield to modern estimates of suspended sediment yield from sediment load monitoring. Results show that the modern estimate for the 2014-2015 season does not differ significantly from the baseline sediment yield. However, this modern estimate does not take into account sediment transported as bedload, which may increase modern sediment yield estimates by 5-50%, and it is based on data collected during a drought period, indicating that modern yields actually exceed the baseline. In addition, aggrading

lower reaches of Fernan Creek indicate an increase in sediment storage, suggesting that modern erosion rates and sediment yields have been enhanced by land use. I have provided a simple and accessible means for estimating baseline erosion for sub-catchments in Fernan, based on the relationship between baseline erosion and basin-averaged slope, to be used in future studies of erosion in the Fernan Creek watershed.

ACKNOWLEDGEMENTS

Funding for this research was provided by Idaho NSF EPSCoR. I would like to thank my advisor Dr. Brian Yanites for his guidance and input throughout this project, and my committee members Dr.'s William Phillips and Frank Wilhelm for their input, suggestions, and guidance. I would like to thank Dr. William Rember for his input on this project and the Fernan community for allowing me to present my research, especially Mike Webb for taking an interest in this research and for providing access to his land for sediment and core sampling. Finally, I would like to thank Jeff Larimer for teaching me the lab procedure for isolating quartz for ^{10}Be analyses.

TABLE OF CONTENTS

Authorization to Submit Thesis.....	ii
Abstract	iii
Acknowledgements.....	v
Table of Contents	vi
List of Figures	ix
List of Tables.....	x
CHAPTER 1: INTRODUCTION	1
1.1 Study Outline	2
CHAPTER 2: METHODS.....	6
2.1 Baseline Erosion Rates	6
Modeling Erosion Rates	7
Model Assumptions	9
Snow Shielding.....	10
Topographic Shielding.....	12
¹⁰ Be Concentration by Grain Size.....	14
Sample Preparation	15
Mixing Models.....	17
2.2 Baseline Sediment Storage	18

Core Extraction, Processing, and Stratigraphic Correlation	18
Age-Depth Model.....	19
2.3 Topographic Analysis of Lidar Data.....	20
Basin-Average Slope	20
Degree of Bedrock Exposure.....	21
CHAPTER 3: RESULTS	22
3.1 Baseline Erosion Rates	22
3.2 Baseline Sediment Storage	22
3.3 Topographic Analysis of Lidar	23
CHAPTER 4: DISCUSSION.....	24
4.1 Baseline Sediment Budget	24
Sediment Storage.....	24
Baseline Sediment Yield.....	26
Comparing Baseline and Modern Sediment Yield Rates	26
4.2 Baseline Erosion and Topography.....	29
CHAPTER 5: CONCLUSIONS	32
REFERENCES	34
FIGURES	45

TABLES63

APPENDIX.....69

LIST OF FIGURES

Figure 1 Regional context of the Fernan watershed	45
Figure 2 Photo of algal blooms in Fernan Lake	46
Figure 3: A map of land use throughout the watershed	47
Figure 4: Photo of the Fernan Creek Road Project material.....	48
Figure 5: Sub-basin considered in this study	49
Figure 6: SNOTEL and SNOLITE site locations	50
Figure 7: Correction factor by elevation	51
Figure 8: A map of snow shielding coefficients	52
Figure 9: A map of topographic shielding coefficients	53
Figure 10: Photo of the Geoprobe coring device.....	54
Figure 11: Figure illustrating the correlation between sediment cores.....	55
Figure 12: The weighted-linear age-depth model	56
Figure 13: Determination of critical slope for REI.....	57
Figure 14: Map of erosion by sub-basin.....	58
Figure 15: Quantified relationship between slope and erosion	59
Figure 16: Map of rock exposure predicted by the REI	60
Figure 17: Graph of the long-profile of Fernan Creek	61
Figure 18: Distribution of slopes by basin.....	62

LIST OF TABLES

Table 1: Erosion Rates from ^{10}Be Concentrations.....	63
Table 2: Erosion Modeling Corrections.....	64
Table 3: SNOTEL Snow-Water Equivalent Data	65
Table 4: Basin B(east) Mixing Model.....	66
Table 5: Basin A(south) Mixing Model	66
Table 6: Carbon-14 Ages	67
Table 7: Basin Characteristics	68
Appendix 1: Photos of Core Segments.....	69

CHAPTER 1: INTRODUCTION

The Fernan watershed is approximately 49 km² of mostly forested, mountainous terrain located in Kootenai County, Idaho. Fernan Creek is the primary stream draining the Fernan watershed and is the major perennial source of water to Fernan Lake, a Pleistocene lake created when gravel and cobble deposits from the Missoula Floods dammed the Spokane River drainage basin. Baseflow for Fernan Creek is below 1 ft³ sec⁻¹, and the hydrology of this stream is driven primarily by runoff from snowmelt, including significant rain-on-snow events which tend to produce spikes in flow during the late winter season (IDEQ 2013).

Over the last two to three decades, the water quality of Fernan Lake has raised concerns from local landowners about suitability of the lake for domestic and recreational use. Cyanobacteria blooms occur seasonally in Fernan Lake from late summer to early fall in response to phosphorus loading of the lake (IDEQ 2013) (Figure 2). These blooms produce thick mats of algae and create toxic water conditions which can be harmful to both humans and pets (IDEQ 2013). As a result, Fernan Lake has been listed on Idaho's §303(d) list of impaired waters for not supporting recreational use (IDEQ 2011). The Idaho Department of Environmental Quality (IDEQ), along with local volunteer organizations and researchers, have worked together to assess the nutrient loading of the lake which has led to the current water conditions.

The IDEQ TMDL (Total Maximum Daily Loads) report (2013) has identified the Fernan Creek watershed as the primary nonpoint source of nutrient pollution and sediment to Fernan Lake. It has been suggested that increased soil erosion, as a result of current land use

practices, has led to increased delivery of fine sediment, which carries phosphorus, to the lake (IDEQ 2013). Specific land use practices cited in the TMDL report include: timber harvesting and road building on Forest Service land in the upper watershed, as well as construction and development on steep slopes in the privately-owned lower watershed (Figure 3). There is additional concern that excess sediment stored along the Fernan Creek channel, from reconstruction of the Fernan Creek road (Figure 4), is being continuously eroded contributing to the poor water quality of Fernan Lake.

These land use practices are believed to have increased soil erosion above the background rate both directly, as well as indirectly as a result of increased runoff due to soil compaction and vegetation removal (Fernan Lake Management Plan 2003). However, to date there has been no effort to quantify the background rate of soil erosion for use in evaluating the impact of these activities. Quantifying a background rate of erosion for the Fernan landscape would allow land managers in Fernan to assess the impact of land use practices on soil erosion by establishing a reference rate to which current erosion rates could be compared. In addition, quantifying the background rate of erosion would provide an opportunity to prioritize the management of sub-catchments throughout the watershed by allowing land managers to compare the extent of impact between sub-catchments.

1.1 Study Outline

For this study I have quantified baseline erosion rates for the Fernan Creek watershed using concentrations of cosmogenic Beryllium-10 (^{10}Be) in alluvial quartz. Cosmogenic ^{10}Be concentrations record the rate of exhumation of quartz grains to the surface, and integrate erosion rates over 10^4 - 10^5 year time-scales (Brown et al. 1995;

Granger et al. 1996; Bierman & Stieg 1996). The long integration period averages over short-term variability in erosion due to changes in land use and variable hydrologic factors. Thus, erosion rates modeled from cosmogenic ^{10}Be provide a good estimate of the long-term average erosion rate, which can be used as a baseline rate for comparison with current erosion rates. I have quantified baseline erosion rates for six sub-basins throughout the Fernan watershed to assess the spatial variability in erosion (Figure 5).

I have also modeled the rate of sediment deposition on the floodplain using Carbon-14 (^{14}C) dates from sediment cores taken from the Fernan Creek floodplain. Because Fernan Creek has an established floodplain, there is some degree of sediment storage which has taken place over the time scales integrated by ^{10}Be concentrations. To directly compare baseline erosion rates to modern estimates of the sediment yield, from sediment load monitoring of Fernan Creek (LaCroix 2015), the baseline rate of sediment storage needs to be accounted for in the sediment budget, which is a quantitative means of addressing sediment production, storage, and yield over time. Expressed in general form the sediment budget is:

$$(1) \text{ Input} - \text{Output} = \Delta\text{Storage}$$

Subtracting the rate of sediment storage from the baseline erosion rate (Input) gives the baseline sediment yield (Output) of Fernan Creek; a sediment yield is a measure of the amount of sediment passing a certain point in a given amount of time. To address sediment storage, I have modeled the change in age with depth in the core profile. I have used this model to quantify an $\sim 11,000$ year average sedimentation rate, which I used to discuss trends in sediment storage and to provide a quantitative estimate of the baseline storage

rate. I compared baseline sediment yield to the modern yield estimate to provide quantitative insight into the extent to which land use has altered soil erosion and sediment transport in the watershed.

Finally, I have quantified topographic metrics, such as basin average slope and the degree of bedrock exposure, for each of the six sub-basins. I compared these topographic metrics to observed erosional patterns to discuss hillslope mechanisms driving erosion throughout the watershed. I have also quantified the relationship between baseline erosion rates and basin-averaged slope to provide an accessible means for land managers to estimate baseline erosion rates for individual sub-basins in the Fernan watershed which were not explicitly looked at in this study. As I have mentioned, these baseline rates can be used to evaluate the extent of land use impact, as well as to prioritize management efforts.

Previous work quantifying cosmogenic ^{10}Be -derived erosion rates has demonstrated the value of comparing erosion rates over multiple time-scales. For instance, Kirchner et al. (2001) showed that modern estimates of erosion, averaged over decadal time-scales, were orders-of-magnitude less than those averaged over millennia (from the cosmogenic approach) in the Idaho batholith, indicating that decadal-scale monitoring underestimates the true sediment delivery. Many similar studies have been done in areas where no long-term sediment storage is observed so that hillslope erosion, converted to an annual sediment flux, may be interpreted as a baseline sediment yield. However, in landscapes with developed floodplains the sediment transported downstream may be restricted during high discharge as overbank flows carry sediment from the channel to be stored on the floodplain surface. Therefore, the sediment yield is less than the soil erosion rate on hillslopes due to a

net sediment storage on the floodplain over the time period integrated by cosmogenic ^{10}Be concentrations. To my knowledge, no studies have quantified a baseline rate of storage to be used for comparison with baseline erosion rates in a sediment budget. To apply the cosmogenic approach to the Fernan landscape, which has a developed floodplain, I have quantified a baseline storage rate using the sediment core method introduced above, and I compare this to cosmogenically-derived erosion rates. This approach provides a means for relating cosmogenic erosion rates to modern sediment yields in landscapes where significant long-term storage is present.

CHAPTER 2: METHODS

2.1 Baseline Erosion Rates

I have modeled erosion rates from cosmogenic ^{10}Be concentrations in alluvial quartz to represent baseline erosion rates for the Fernan landscape. Cosmogenic ^{10}Be is produced in quartz primarily by spallation reactions, when high-energy particles bombard oxygen-16 (^{16}O) atoms causing them to fragment. To a lesser degree, ^{10}Be is produced by fast and slow muon capture. The basic idea behind modeling erosion rates from these concentrations is that cosmogenic ^{10}Be is produced in quartz at a constant rate from exposure to cosmic radiation, which attenuates below the surface as a function of material (rock) density (Lal 1991). Quartz is effectively shielded from exposure to cosmic rays below ~ 2 meters from the surface. Therefore, by measuring the concentration of ^{10}Be in sediment at the surface, it is possible to infer the time of near-surface exposure, which depends on the rate of erosion (Granger et al. 1996; Brown et al. 1995; Bierman & Stieg 1996).

A spatially-averaged erosion rate can be inferred from the ^{10}Be concentration of a quartz sample collected from the stream sediment at a basin outlet. It is assumed that each region of the landscape has contributed sediment to the stream channel in proportion to its erosion rate, and that hillslope and fluvial transport has thoroughly mixed this sediment. When these conditions are met, sediment sampled from the channel at a basin outlet is representative of the entire landscape upstream from the sample location. The ^{10}Be concentrations of individual quartz grains from this sample have recorded exhumation rates from each individual region of the landscape. Because the sediment is well-mixed, the ^{10}Be concentration measured from the collection of quartz grains in this sample is representative

of the average exhumation rate of these grains. Therefore, it is possible to model a spatially-averaged erosion rate from this concentration using a basin-averaged rate of ^{10}Be production (Brown et al. 1995; Bierman & Stieg 1996; Granger et al. 1996; von Blanckenburg 2005).

This method has been tested by both Granger et al. (1996) and Brown et al. (1995). Specifically, Granger et al. (1996) tested the validity of the model by comparing estimates of erosion rates from ^{10}Be concentrations to alluvial fan accumulations rates. They found that the two rates were generally consistent (within \sim one standard error), indicating that concentrations of ^{10}Be in alluvial sediments can be used to estimate the pace of landscape erosion.

Modeling Erosion Rates

To infer erosion rates from ^{10}Be concentrations, I have used the analytical model from Granger et al. (1996) and Brown et al. (1995). This model uses the attenuation of cosmic rays below the surface to calculate erosion rates. For a flat surface exposed to cosmic rays, the production of ^{10}Be attenuates with depth according to the equation:

$$(2) P(z) = P_0 e^{-\rho z/\Lambda} \quad (\text{Lal 1991})$$

Where, P is the production rate ($\text{atoms g}^{-1} \text{yr}^{-1}$), z is the depth below the surface, P_0 refers to production at the surface, ρ is the mean density of rock (g cm^{-3}), and Λ is the effective attenuation length (160 g cm^{-2} , Gosse & Phillips 2001). The equation above assumes that the surface production rates at a location do not vary over time.

For constant erosion, grains of quartz are steadily brought to the surface, accumulating ^{10}Be at a rate defined by their depth and equation 2. The rate that grains move

along the attenuated production curve (equation 2), toward the surface, is determined by the erosion rate. Therefore, concentrations of grains at the surface reflect the average erosion rate integrated over the period that grains spent within 2 meters of the surface. Due to the long half-life of ^{10}Be (1.387 ± 0.012 My, Chmeleff et al. 2010), the effect of radioactive decay on ^{10}Be concentrations in grains exhumed to the surface is negligible for moderate to high erosion rates. Basin-wide long-term erosion can be modeled as:

$$(3) E = \frac{\Delta P_0}{\rho N}$$

Where, E is erosion (cm yr^{-1}) integrated over the time to erode the upper two meters, and N is measured concentration (atoms g^{-1}). However, modeling erosion rates according to equation 3 assumes that ^{10}Be is only accumulated during the exhumation of quartz grains. This is clearly not the case for sediment sampled at a basin outlet, as quartz grains are exposed to cosmic radiation during transport and storage. The increase in concentration will have a negligible effect on inferred erosion rates as long as sediment storage and transport times are significantly less than the time that grains are exposed during exhumation (Granger et al. 1996). Further assumptions of the model are considered in the next section.

The production rate of cosmogenic ^{10}Be varies as a function of both altitude (air pressure) and latitude. It is therefore necessary to determine site-specific surface production rates for the Fernan watershed before modeling erosion rates. Here, I have determined surface production rates from Hidy (2013) (both spallogenic and muogenic) pixel-by-pixel from 1-meter Lidar of the Fernan watershed. Per-pixel ^{10}Be production rates are based on a reference rate scaled to the latitude and elevation of each pixel according to the scaling relationships determined by Stone (2000). I used basin-averaged production rate values in

the model above (equation 3) to infer erosion rates for each of the tested sub-basins. I have excluded production rates corresponding to the area of the floodplain from basin-averages because the floodplain experiences a net storage and thus does not contribute sediment according to the model.

Model Assumptions

In general, the concentration of ^{10}Be in sediments leaving a basin is inversely related to the average rate of erosion (Bierman & Stieg 1996). Modeling basin-wide erosion rates from these concentrations assumes several conditions. First, the model assumes that alluvial sediment samples are well-mixed and representative of the catchment as a whole.

Additionally, it assumes that the transport and storage times of sediment on hillslopes are short in comparison to the erosional time scale (i.e. the time it takes to exhume sediment through the $1/e$ attenuation length for surface production rates) (Granger et al. 1996).

Additional factors which may complicate the interpretation of erosion rates from ^{10}Be concentrations include: glaciation, snow-shielding of the surface (Schildgen et al. 2005), topographic shielding of the surface (Codilean 2006; Gosse & Phillips 2001), landsliding (Yanites et al. 2009), and an uneven distribution of quartz throughout the watershed (Bierman & Stieg 1996).

Many of these complicating factors can be dismissed through analysis of the landscape. For instance, there is no evidence from the topography of the Fernan watershed of recent deep-seated landslides which contribute low-dosed sediment to the channel, skewing modeled erosion rates. The steep terrain and steep drainage network of Fernan, comprised of mostly low-order streams, support the assumption that transport and storage

times are probably low compared to the erosional residence time. Significant storage times of sediment on the floodplain should not affect results, because sediment stored on the floodplain is generally finer-grained than the sand and gravel size fractions I have sampled for ^{10}Be analyses. Finally, it is reasonable to assume that sediment mixing is sufficient at the sample locations, because sediment has been sampled from low areas in the sub-basins, far from main tributary junctions, and localized sources of sediment input from hillslopes (Binnie et al. 2006). The remaining complicating factors cannot be so readily dismissed and are addressed in the following two sections.

Snow Shielding

Snow cover has an attenuating effect on cosmic ray intensity, lowering production rates of ^{10}Be at the soil surface. Erosion rates can be over-estimated if quartz shielding due to snow cover is not accounted for. In similar studies, snow shielding has been addressed by correcting surface production rates by >10% (Schildgen et al. 2005), and possibly up to 40% (Zweck et al. 2013). Previous corrections have been based on either snow-cover data from monitoring programs encompassing a few decades of climatic variability, or longer-term Holocene climate modeling. For this study, I have determined snow shielding of quartz based on the Natural Resource Conservation Service (NRCS) SNOTEL snow-water equivalent data. This data has been taken from eight sites in close proximity to the Fernan watershed (Figure 6).

As I discuss in above, the attenuation of cosmic ray intensity is determined by the density of material through which the rays travel. Snow density is determined by the amount of liquid water it contains, which is called the “snow-water equivalent” (SWE). For a given

depth of snow cover, the attenuation of ^{10}Be production through its equivalent SWE depth is given by:

$$(4) P(s) = P_{\text{raw}}e^{-\rho s/\Lambda}$$

Where ρ is the density of liquid water (g cm^{-3}), s is the SWE depth (cm), $P(s)$ is the production rate ($\text{atoms g}^{-1} \text{yr}^{-1}$) at the soil surface, and P_{raw} refers to the raw production rate scaled to latitude and elevation.

Dividing both sides by P_{raw} gives the ratio of attenuated production to raw production. This value, which I have called the “correction factor” (CF), represents the fraction of the surface production rate that is effective at the soil surface. The CF is given by:

$$(5) \text{CF} = e^{-\rho s/\Lambda}$$

Multiplying this factor by P_0 yields a surface production rate which takes into account the shielding of quartz grains due to snow cover.

I have compiled 30-year (1981-2010) monthly median SWE values from NRCS SNOTEL and SNOLITE data (Table 3). This data has come from eight locations surrounding the Fernan watershed, which vary within approximately one-third of a degree in latitude. The elevation range of these sites approximates the range in elevation of the Fernan watershed. I calculated the mean annual SWE depth, in cm, from monthly (30-year) median values for each elevation and considered this value to be a constant attenuating depth of water for an entire year. Then, I calculated the CF for each of these elevations using the mean annual SWE value for “ s ” according to equation 5 above. I fit a linear model to this data to represent CF by elevation (Figure 7), and calculated the CF for each pixel from 1-meter elevation data

for the Fernan watershed using the equation of the linear model (Figure 7). Finally, I averaged pixel CF values within each basin to correct surface production rates.

As a final note, residence times calculated from uncorrected erosion rates (in Fernan) indicate that these rates are integrated over time scales ranging from ~8-20 ky, which extends into the Last Glacial Maximum. The Fernan landscape may have been subject to increased snow cover during the LGM and more variable snow cover throughout the early to middle Holocene. Therefore, I conclude that the snow shielding factors which I present here represent a minimum estimate of long-term shielding.

Topographic Shielding

The effective production rate of a point on a hillslope surface is further influenced by the landscape topography. Topography reduces exposure to cosmic rays in two ways: First, the surrounding topography can intercept incoming radiation before it reaches another point. Second, points located on steep slopes receive less radiation due to the near-vertical angle of incidence of incoming radiation and the foreshortening effect (see Gosse & Phillips 2001). These factors decrease the effective surface production rates and, if they are not accounted for, will lead to further overestimation of erosion rates from ^{10}Be concentrations.

The common method for determining topographic shielding at a single site is to record the azimuth and slope at the site and determine the elevation angles (elevation above the horizontal plane intersecting the sample site) of different topographic features obstructing the horizon (Gosse & Phillips 2001). For single points on a landscape this method may be effective, but it quickly becomes labor intensive as entire basins are considered. To address this issue, Codilean (2006) proposes the use of digital elevation model (DEM)

hillshading. A hillshade map is a grayscale representation of a surface which takes into account the position of pixel in relation to the location of a single light source to calculate illumination values. Codilean (2006) has suggested that shielding at each location on a landscape can be determined by varying the position of the light source (both its elevation angle and azimuth) incrementally. Topographic shielding is determined by averaging the illumination values of each pixel for all positions of the light source and dividing by the maximum value.

I have used the method described above from the automated toolbox produced by Li (2013) (downloaded from web.utk.edu/~yli32/) to quantify basin-averaged values of topographic shielding. The output of this function yields pixel values between 0 and 1, representing the shielded fraction of incoming radiation. Subtracting this value from 1 yields the fraction of total radiation reaching each point (equivalent to the CF from snow shielding). I used 1/3 arc-second digital elevation data (USGS, NED) to calculate topographic shielding coefficients for each pixel (Figure 9). I calculated basin-average values of pixel shielding for each sub-basin to account for the spatially averaging nature of basin-wide erosion rates from ^{10}Be .

One limitation to this method that I can envision, is the negative shielding factor associated with interception of cosmic rays. When a location on the landscape is shielded, the surrounding topography receives a higher proportion of incoming radiation, implying a negative shielding coefficient. Therefore, if the majority of interception occurs within a basin, the basin-averaged shielding coefficient will be effectively zero. The effective shielding coefficients then depend on the amount of radiation intercepted outside of the basin. The

hillshade method does not address the location of topography obstructing incoming radiation and is therefore limited in its capacity to predict shielding coefficients. I have included this method in my analysis to discuss the full range of modeled erosion rates, but I acknowledge that actual topographic shielding may be less than that calculated here.

¹⁰Be Concentration by Grain Size

Along with modeling erosion rates from ¹⁰Be in alluvial sand, some researchers have tested the dependence of ¹⁰Be concentrations on grain size in an effort to further explain erosional processes at work, and accurately determine long-term erosion rates (Aguilar et al. 2014; Belmont et al. 2007; Brown et al. 1998; Matmon et al. 2003; Puchol et al. 2014). Tests of concentration by grain size are based on the idea that lower concentrations indicate that sediment was derived from greater depth. Thus, significantly lower concentrations in larger grain size fractions indicate rapid transport of relatively un-weathered sediment to the surface by deep erosional processes (e.g. shallow landslides).

In several published cases, ¹⁰Be concentrations of gravel have been shown to be less than those of sand (Aguilar et al. 2014; Belmont et al, 2007; Brown et al, 1998; Matmon et al, 2003; Puchol et al, 2014). Aguilar et al. (2014) have suggested that the concentrations in sand are determined by the mean denudation rate, while concentrations in gravel are determined by the frequency of hillslope failure. By comparing concentrations between grain sizes, it is possible to infer the erosional mechanisms responsible for creating apparent contrasts.

Here I have measured ¹⁰Be concentrations of gravel for basins A, C, and D for comparison with sand. To evaluate potential mechanisms responsible for contrasts by grain

size, I determined the depths from which gravel samples were derived for a given difference in concentration. I modeled concentrations with depth for an eroding landscape according to the equation:

$$(6) \quad dN(z) = (-N(z)\lambda + P(z))dt \quad (\text{Lal 1991})$$

Where λ is the decay constant for ^{10}Be , and t refers to time (years). I have used the modeled erosion rates from ^{10}Be concentrations in sand samples to define the rate at which model grains move towards the surface. I ran the model until ^{10}Be concentrations at the surface reached equilibrium with the erosion rate, and then I determined the average depth of gravel samples based on the concentration profile below the surface.

Sample Preparation

For this study, I have collected alluvial sediment samples from 4 sites throughout the watershed and wet-sieved these samples to collect grain size fractions from 250-500 μm . I have also taken gravel samples from material collected by the coarsest sieve (>1670 μm) and crushed them for processing. To ensure that there was no remaining fine sediment that may have been aerially deposited, I washed the samples with deionized (DI) water and dish soap. I then isolated quartz from these samples using similar methods to those outlined by Kohl & Nishiizumi (1992). This method involved etching samples in diluted 12 N HCl on a hot plate for 24 hours to eliminate carbonates and organic material. Then, samples were leached in a 5% HF/HNO₃ solution for four rounds, the first on hot-dog rollers and final three in an ultrasonic bath (for agitation). Leaching eliminates most silicate minerals other than quartz and dissolves the weathered rind of quartz, which contains meteoric ^{10}Be . I removed remaining heavy minerals using Lithium Metatungstate (LMT), a dense liquid, which allowed

quartz to float as heavier minerals settled out. I separated remaining light minerals from quartz samples by adjusting the density of LMT, by adding DI water, to the point that quartz settled out and remaining light minerals floated on top. Magnetic separation of minerals by both a hand magnet and Frantz magnetic separator yielded no magnetic material for two samples and was not attempted on the rest.

Chemical preparation of quartz samples, at the Purdue Rare Isotope Measurement Laboratory (PRIME Lab), included dissolving weighed quartz samples in a concentrated HF/HNO₃ solution, and spiking samples with a known amount of ⁹Be carrier. H₂SO₄ was added to the dissolved samples, and the liquid was evaporated off by high-temperature fuming. Beryllium hydroxides were precipitated out in a high pH solution and washed with deionized water. Solids were dissolved in oxalic acid and Be²⁺ was separated using cation exchange columns to remove any remaining Al, Fe, and Ti oxalates. Beryllium was precipitated a second time in a high pH solution as beryllium hydroxide, washed in DI water, and then dried to convert to beryllium oxide. The final beryllium oxide compound was mixed with niobium (Nb) powder and loaded into a cathode, which is inserted into the accelerated mass spectrometer for analysis.

The ratios of ¹⁰Be/⁹Be were measured at Purdue University by accelerated mass spectrometer. Initial concentrations of ¹⁰Be were calculated assuming a constant ratio throughout chemical preparation of samples. We used the known amount of ⁹Be carrier added at the beginning and the measured ratio of ¹⁰Be/⁹Be to calculate the initial amount of ¹⁰Be for each sample. We divided the measured quantities of ¹⁰Be by the mass of the initial samples to determine ¹⁰Be concentrations (in atoms ¹⁰Be/g SiO₂). In addition, a chemistry

blank was used to determine if any contamination from ^9Be occurred during sample processing. Further information on PRIMELab procedures and the accelerated mass spectrometer used can be found at the PRIMELab website (science.purdue.edu/primelab).

Mixing Models

Sediment at and below tributary junctions is a mixture of sediment from multiple sub-basins upstream. Each of the upstream sub-basins contribute sediment in proportion to their erosion rate and area. Therefore, the total sediment flux leaving the landscape is the sum of each of the individual sub-basins. In the case where erosion has been modeled for both a larger area and some sub-section of that area, the erosion rate corresponding to their difference can be inferred using a mixing model. This works by calculating the difference between sediment fluxes of both basins, and dividing by the difference in their areas.

Formally, this can be expressed as:

$$(7) E_i = (E_{\text{total}}A_{\text{total}} - E_{\text{sub}}A_{\text{sub}})/(A_{\text{total}} - A_{\text{sub}})$$

Where E and A refer to the erosion rate and area of the total landscape and the sub-section.

Basin A encompasses the entirety of the tested watershed, including basins B, C, and D. I have applied a mixing model using the modeled erosion rates and sub-basin areas (equation 7) to determine the erosion rate corresponding to the southern region of basin A, which is basin A(south). Similarly, I calculated the erosion rate for the easternmost section of basin B (basin B(east)). Maps of basins A(south) and B(east) can be seen in Figure 5. The larger errors associated with these erosion rates are the result of propagating error from measured concentrations through the mixing models.

2.2 Baseline Sediment Storage

Core Extraction, Sample Processing, and Stratigraphic Correlation

Northern Lights Drilling LLC extracted two adjacent cores from the lower Fernan Creek floodplain using a Geoprobe coring device (Figure 10). Both cores were taken to a maximum depth of 9.8 meters (32 ft) in 1.2-meter segments. I measured volume magnetic susceptibility (VMS) at 5-cm intervals for each of the two cores using a handheld Kappmeter. I determined the bulk density by sampling a measured volume of sediment where layer properties, such as deposit grain size or color changed. Then, I dried these samples under a heat lamp for up to a week. I weighed the dry samples on a pre-tared watch glass and divided the mass by the measured volume to determine the sample bulk density.

I measured the organic content of deposits throughout the core by the wet oxidation method, using sodium hypochlorite as the oxidizing agent (Siregar et al., 2005). First, I adjusted household bleach (sodium hypochlorite) to pH 9 using 0.5 M HCl, and soaked the samples in this solution to oxidize organic matter. The samples soaked for 1-hour, 30 minutes, 30 minutes, and 15 minutes for each of four successive rounds. After each round, the samples were centrifuged at 2000 rpm to consolidate solid material before pouring off the supernatant. Between rounds, the samples were rinsed with DI water, and centrifuged again before pouring off liquid. The percent organic content is the difference in mass between the initial and bleached samples divided by the initial mass. I used these three properties (VMS, bulk density, and organic content) to correlate stratigraphic layers between cores. Layers were correlated visually by matching trends in each of these properties with

depth. I developed a correlated core sequence, adjusting the depth of sampled carbon based on the correlation (Figure 11).

To quantify the sedimentation rate with time, I took 11 samples of organic matter, both bulk carbon and plant material, throughout the longer of the two cores. Sample processing and analysis of carbon-14 (^{14}C) was done at the University of Arizona in Tucson, Arizona. Results from the tests included both ^{14}C ages and their associated error. Using this data, I constructed an age-depth model to quantify rates of sedimentation over a period spanning the ~11,000 years.

Age-Depth Model

I modeled sediment age in relation to depth below the surface to quantify trends in sedimentation rate from ^{14}C ages distributed throughout the core profile. First, I calibrated ^{14}C dates to years before present (yr. BP), using the INTCAL13 dataset by Reimer et al. (2013). I used the downloadable version of CALIB 7.1 (Stuiver et al., 2005) for calibration. I ran ^{14}C dates and their associated 2-sigma error in CALIB, producing a probability distribution of dates in yr. BP for each sample. Before modeling the age-depth relationship I assessed data for potential outliers. I looked for re-worked samples whose ages were significantly older than those of the surround samples. The single outlier I found was defined by an anomalously old calibrated date relative to its stratigraphic position in relation to other samples. This old date suggests that the sample was not deposited immediately after the plant tissue had died. I removed this outlier before modeling the age-depth relationship.

The distribution of uncertainty when calibrating ^{14}C dates is often non-normal as a result of fluctuations in ^{14}C in the atmosphere over time (Goslar et al. 1995). As a result,

modeling age-depth relationships is difficult because neither the mean nor the median age serves as good point estimate for the distributions. To overcome this limitation, researchers have suggested several statistical methods, from Bayesian statistics (Ramsey 2008, 2009) to more “classical” methods involving linear interpolation and regression (Blaauw 2010). Here, I used a Monte-Carlo “bootstrapping” method similar to Higuera et al. (2009) and the MCAgeDepth program (Higuera 2008).

I used the 10 samples from the core and the radiocarbon date of the Mount Mazama eruption from Hallet et al. (1997). I entered the radiocarbon dates into CALIB (see above) to determine the calibrated age distributions for each sample. Then in Matlab, I sampled calibrated dates randomly from the probability distributions of each sample 10,000 times. After each round I fit a linear model to the random sample selections, weighting the linear model according to the inverse of the standard deviation of the original calibrated date distributions. This means that distributions with higher uncertainty have a lower impact on the model than those with lower uncertainty. I plotted each of these linear models together to represent error bars for the modeled relationship (Figure 12). Finally, I used the median value from each of the sampled distributions to determine the sedimentation rate.

2.3 Topographic Analysis of Lidar Data

Basin-Average Slope

I calculated per-pixel slope values from 1-meter Lidar data for the entire watershed. From this data, I determined basin-average slopes for each of the tested sub-basins. I excluded the floodplain area from slope calculations to ensure that slope values are representative of hillslope processes. To determine the significance of the difference in

mean values, I used a two-tailed hypothesis test ($\alpha = 0.05$, z -value = 1.65) using the basin-average slope values and standard deviations of per-pixel slope distributions.

Degree of Bedrock Exposure

I used a slope-based metric similar to the rock exposure index (REI) by Dibiase et al. (2012) to quantify rock exposure for each sub-basin. This method is based on the premise that, above a certain slope the downslope transport of sediment is instantaneous and sediment does not accumulate. I tested several hillslope angles ranging from 30 to 50 degrees to determine the critical slope angle using a logical expression in ArcGIS 10.1 (Figure 13). I used focal statistics to represent the fraction of rock exposure within a circle of 3-meter radius for each pixel, and evaluated the accuracy predicted outcrops by comparing a raster image to outcropping observed in the field and apparent from Lidar. Then, I calculated the degree of rock exposure for each sub-basin using the mean value of the logical expression. I excluded a 20-meter buffer of the Fernan Creek road from calculations of basin-average rock exposure to avoid the influence of road cut-slopes. This mean value corresponds to the fraction of total basin area above the critical slope value.

CHAPTER 3: RESULTS

3.1 Baseline Erosion Rates

Erosion rates modeled from ^{10}Be concentrations of sand range from 0.031 ± 0.002 mm yr^{-1} to 0.067 ± 0.005 mm yr^{-1} (Figure 14). Corrections for snow shielding and topography alter modeled erosion rates by $\sim 5\text{-}10\%$. In general, erosion rates are lowest in the two upper tributary basins (C and D) and are higher along the main Fernan Creek channel. The highest erosion rate is found in basin A(south), the furthest downstream and closest to the lake.

For basins A and D, ^{10}Be concentrations are dependent on grain size, with larger grain sizes corresponding to lower concentrations. In basin C concentrations between grain sizes showed no significant difference ($\alpha = 5\%$, $z\text{-value} = 1.65$). Modeling indicated that gravel from basin A was derived from an average depth of 19 cm while gravel from basin D was derived from 32 cm. Erosion rates from all sub-basins can be found in Table 1.

3.2 Baseline Sediment Storage

The weighted linear model based on median calibrated dates from Monte-Carlo simulations indicates that the long-term average sediment deposition rate on the floodplain is 0.656 mm yr^{-1} . This model has an R-squared value of 0.98 ($p\text{-value} < 0.05$), indicating that the linear model explains most of the variation in the calibrated age data. The high R-squared value also indicates that the sediment deposition rate has remained relatively constant over the last $\sim 11,000$ years. The intercept of the linear model predicts a date for the modern floodplain surface of 2016, which is one year different from the date when cores were extracted.

3.3 Topographic Analysis of Lidar Data

Basin-average slope values fell between 21.3 and 24.7 degrees, corresponding to a range of 3.4 degrees. The standard deviations of slope ranged from 7.1 to 8.7 degrees. The difference between mean slope values were significantly different from one another according to a z-test ($\alpha = 5\%$, $z\text{-value} = 1.65$). Basin-average slopes exhibit the same general trend as erosion rates, with lowest values in the upper tributary basins (C and D) and higher values along Fernan Creek. In general, erosion rates are positively correlated with both mean and median slope values ($R^2 = 0.72$ and 0.82 respectively) for basins C, D, A(south), and B(east). However, basin B(east) has the highest mean and median slope while its erosion rate is less than that of A(south). Erosion is not strongly related to Pearson's Skewness Index or the standard deviation of slope. However, both mean and median slopes are strongly positively correlated with the standard deviation of slope ($R^2 = 0.96$).

Rock exposure predicted by the REI accounts for less than 1% of the total watershed area. Rock exposure in basin B(east) is over twice that of the rest of the watershed (REI = 0.41%) For basins C, D, and A(south) rock exposure increases semi-linearly with erosion rate. However, a large spike in REI for basin B(east) does not correspond to an increase in erosion. Rock exposure does not appear to be strongly correlated with either mean or median slope, or distribution skew, but it is positively correlated with the standard deviation of slope ($R^2 = 0.82$).

CHAPTER 4: DISCUSSION

4.1 Baseline Sediment Budget

Sediment Storage

According to the weighted linear age-depth model (p -value < 0.05 , $R^2 = 0.98$), the sedimentation rate of the floodplain has not varied significantly over ~11,000 years.

However, the rate of sediment storage has likely increased over time due to the development of the Fernan Creek floodplain. Following the creation of the lake 15-12 ka (Hanson et al. 2011), the water level of Fernan Lake rose its current level and the current floodplain area was probably underwater. The east end of Fernan Lake filled in over time until it rose above the lake level, creating the floodplain, while the eastern end of the lake continued to fill in. This means that the area of the floodplain has increased over time while the lake area has shrunk in response.

The sedimentation rate I have quantified represents the rate at a single point on the floodplain. However, previous studies such as Walling (1998) have examined the pattern of variability in overbank sedimentation on the floodplains of rivers in the United Kingdom. Walling (1998) found no streamwise variation in sedimentation, which he attributed in part, to the short length of the studied reaches. In addition, it was shown that sedimentation rate decreases with lateral distance from the stream channel. The section of Fernan Creek channel which winds through the floodplain is an approximately 5 km reach which is about half the length of those of interest in the study mentioned above. For that reason it is reasonable to suggest that there is no consistent trend in sedimentation with distance downstream. However, it is reasonable to assume that there is significant lateral variation in

sedimentation resulting from coarser grains settling out over shorter distances from the channel onto the floodplain. But, the sedimentation rate that I have quantified spans approximately 11,000 years. The meandering nature of Fernan Creek throughout the floodplain suggests that the position of the channel has occupied several locations throughout 11,000 years. This means that a decreasing trend in sedimentation rate with distance from the channel should be averaged over as each point on the floodplain has inhabited a number of distances from the channel over 11,000 years. For these reasons, it should be fair to suggest that the sedimentation rate that I have modeled represents a reasonable approximation of the average sedimentation rate of the entire floodplain.

Making the simplifying assumptions that the baseline sedimentation rate is uniform throughout the floodplain, and constant over time, means that baseline sediment storage can be calculated as the product of the floodplain area and the deposition rate. Because the sedimentation rate is apparently constant with time, as indicated by the age-depth model, the sediment budget equation can be re-written as:

$$(8) \text{ Input} - \text{Output} = R \times \text{Floodplain Area}$$

Where R here is the sedimentation rate and is a constant. I have explained that the floodplain area has increased over time, and for a constant sedimentation rate this means that storage has increased at a steady rate over time. This indicates that either: Input (hillslope erosion) has increased as sediment delivery to the lake has remained constant, or that delivery to the lake has decreased over time in response to a growing floodplain and shrinking lake. While an increase in erosion rate cannot be ruled out because no quantitative studies have looked at sedimentation trends throughout the Holocene for this region, it is

more feasible that sediment storage has increased as the floodplain area has grown over time. This suggests that sediment delivery to the lake has decreased over the 11,000 year period at a rate determined by the rate of floodplain growth. In addition, this means that the baseline storage rate for the current conditions can be calculated by multiplying the current area of the floodplain by the constant rate of deposition. This corresponds to an annual sediment flux into storage of 1,810 tonnes yr⁻¹.

Baseline Sediment Yield

According to the sediment budget, the baseline sediment yield is the sediment flux into storage subtracted from the sediment flux from the eroding landscape (Input). The sediment flux from the landscape, determined as the product of the baseline erosion rate and area of basin A, is 4,250 ± 235 tonnes yr⁻¹ using the uncorrected erosion rate. Factoring in corrections for topographic and snow shielding of quartz in the erosion model reduces this yield to 3,910 ± 235 tonnes yr⁻¹. Finally, subtracting the baseline storage rate gives an annual yield of 2,440 ± 315 tonnes yr⁻¹ based on uncorrected erosion rates, or 2,100 ± 235 tonnes yr⁻¹ factoring in corrections.

Comparing Baseline and Modern Sediment Yield Rates

From April 2014 to April 2015 suspended sediment load was monitored in Fernan Creek just upstream from Fernan Lake (LaCroix 2015). Suspended load was determined from measurements of total residue (TR), which were regressed with flow discharge so that discharge monitoring could be used to predict TR. The results showed that the area corresponding to basin A produced an annual sediment yield of 2,040 tonnes yr⁻¹. Within the

monitoring period, 29% of the total annual load was delivered to Fernan Lake during the month of February.

Comparing this modern estimate to the baseline sediment yield shows that baseline rates are higher than the modern sediment yield. However, the modern sediment yield falls within the analytical uncertainty (propagated from ^{10}Be measurements) of both the corrected and uncorrected baseline yields. Therefore, the modern yield is not significantly different from the baseline.

There are a few additional factors to take into account when comparing these two rates. First, the modern sediment yield estimate was based on data collected during a drought year. While significant amounts of sediment were delivered to the lake during the month of February, the rest of the year likely represents a lower than average sediment yield. The effect of land management on soil erosion and sediment transport during this period is likely minimized in the modern sediment yield estimate due to decreased runoff and below average discharge in Fernan Creek. This suggests that the modern sediment yield in an average water year would likely exceed the baseline rate.

It is also important to note that estimates of sediment yield from LaCroix (2015) only account for material transported as suspended load. Bedload would need to exceed 10% of the annual sediment load to exceed the upper limit of uncertainty in baseline yields. Sediment load data from Mueller and Pitlick (2013) indicate that bedload accounts for 5-50% (mean of 29%) of annual sediment loads in watersheds near Fernan of similar size, lithology, and climate. This also suggests that the modern annual sediment yield rates exceed baseline yields.

Finally, a study by Kirchner et al. (2001) suggests that the majority of sediment in mountainous terrain is transported during high-magnitude events which can occur decades to centuries apart. Stream monitoring by LaCroix (2015) was done over the course of a single year, and therefore probably did not capture the delivery of sediment by these large events. While the annual yield rate for the month of February was more than 12x the background rate, it is unlikely that this event was one of the large magnitude events referred to by Kirchner et al. (2001), especially because it occurred during a drought year. These additional factors indicate that modern sediment yields for the watershed exceed the baseline, likely reflecting the impact of land management on soil erosion.

Even if I consider the modern sediment yield to be approximately equal to the baseline yield, aggrading lower reaches of Fernan Creek suggest that soil erosion has been increased above the baseline rate. According to the sediment budget equation, if two sediment yields (outputs) are the same, and it is hypothesized that hillslope erosion rates (inputs) are the same, there should be no change in sediment storage for the hypothesis to be true. However, in the "2013 Fernan Lake Addendum" (IDEQ 2013), the IDEQ discusses issues associated with aggrading lower reaches of Fernan Creek. Sediment deposition within the channel in these reaches has raised the bed elevation, lowering the channel capacity and increasing the frequency of flooding (IDEQ 2013). This suggests that modern storage of sediment has been increased above baseline storage rates, which further implies that there has been an increase in sediment supply from soil erosion on hillslopes.

To conclude, the modern sediment yield falls within the uncertainty of the baseline yield. However, the modern yield is based on suspended load estimates only, and was also

based on data collected during a drought period. Additionally, the data was collected over a single year and therefore probably does not reflect the transport of sediment during infrequent high-magnitude events. Furthermore, the aggrading lower reaches of Fernan Creek suggest an increase in sediment supply from hillslopes, likely reflecting the influence of land management in the upper watershed. Therefore, it is rational to conclude that soil erosion on hillslopes has been enhanced by land use contributing to high sediment delivery to the lake, as well as increased flooding frequency on the floodplain. It is feasible to suggest that increased sediment delivery to Fernan Lake from land use practices has led to excess nutrient delivery, which has contributed to the poor water quality in the lake. I cannot, however, point to a specific land use practice, such as logging or road building, which has led to the increase in erosion. For further study in Fernan, I would suggest that a sediment monitoring be put into place to quantify sediment yield for watershed as well as several smaller sub-catchments. The monitoring program should collect data for longer periods (several years) to encompass a wider range of climatic variability to assess the full extent of impact. Monitoring several small sub-catchments would allow managers to compare the impact between sub-catchments to prioritize management efforts. Then, efforts such as surveying roads for erosion could be directed more efficiently and would help to further identify erosion “hot-spots” which could be managed more intensely.

4.2 Baseline Erosion and Topography

Erosion modeled from cosmogenic ^{10}Be is positively correlated with mean slope for basins C, D, A(south), and B(east) ($R^2 = 0.72$). The regression equation for this relationship is:

$$(9) \text{ Erosion} = -0.1190 + 0.00722 \times \text{Slope}$$

Where Erosion is in mm yr^{-1} and Slope is basin-averaged slope in degrees. This equation suggests that erosion goes to zero when the mean slope is below 16 degrees based on the relationship between the four sub-basins. This equation can be used to estimate baseline erosion for sub-basins that I have not explicitly addressed within the Fernan Watershed.

However, as I explained in the Results chapter, basin B(east) has the highest mean slope value but its erosion rate is less than basin A(south). Therefore, it does not strictly conform to the trend of equation 9 above. This deviation cannot be attributed to long storage or transport times of sediment because basin A(south), located lowest in the watershed, would be affected most by long storage and transport times indicating that the actual erosion rate in basin A(south) is even higher. This would increase the non-linearity of the trend. The deviation from the trend is also not the result of corrections for snow or topographic shielding, as these correction have had minimal effect on erosion rates.

Similarly, the observed relationship between erosion and slope cannot be attributed to an increasing reliance on weathering-limited processes. If sediment transport outpaces sediment production from weathering bedrock, erosion is said to be weathering-limited, and bedrock outcropping would be exposed. The REI shows that bedrock exposure accounts for less than 1% of the total watershed area, and that outcrops are limited to steep slopes along the Fernan Creek channel (Figure 16). The REI did not correlate with any of the slope metrics except the standard deviation, indicating that increased outcropping has led to a wider distribution of slopes while not increasing the overall mean slope. The majority outcropping does appear to correspond to the same area as a knickpoint in Fernan Creek (Figure 17),

which suggests that the main channel may be incising and would explain the higher erosion rates along the Fernan Creek channel.

There is however at least one explanation for why the erosion rates do not increase more linearly with increasing slope. Other studies which have examined the relationship between erosion and slope have shown that erosion increases linearly with slope for small mean hillslope gradients but beyond this point, erosion either increases exponentially with slope (Granger et al. 1996) or becomes decoupled from slope (Binnie et al. 2007; DiBiase et al. 2010). The common explanation for this phenomenon is that erosion on shallow slopes is controlled by surface processes which transport sediment according to linear diffusion (i.e. tree throw, burrowing, rain splash, etc) while at higher slopes near the critical angle of stability for sediment, erosion is dominated by processes such as shallow landslides or debris flows and depend less on slope. Therefore, the deviation from a strictly linear relationship between erosion and mean basin slope may reflect a difference in the processes driving erosion.

To conclude, the modeled erosion rates increase at least semi linearly with increasing slope. The regression equation for this relationship is shown above. This equation can be used to estimate baseline erosion for sub-basins in Fernan based on their basin averaged slope. The actual relationship does strictly adhere to the modeled relationship. This likely reflects a difference in surface processes driving erosion. Regardless, equation 9 above should provide a good estimate of baseline erosion for the Fernan watershed. Care should be taken however, when predicting erosion from slope values which fall outside the range considered in this study.

CHAPTER 5: CONCLUSIONS

It is clear from the data and evidence that I have presented here, that soil erosion and sediment transport processes in the Fernan watershed have been influenced by land management. The modern sediment yield estimate accounts only for suspended sediment, ignoring sediment transported as bedload, and was based on data collected during a drought year. Despite that, the modern estimate is similar, if not equal to, the baseline sediment yield rate. In addition, the modern aggrading lower reaches of Fernan indicates an increase in sediment supply from upstream.

I have quantified the baseline rates of erosion in Fernan and have quantified the relationship between these erosion rates and mean slope to establish a means of estimating baseline erosion for individual regions of the Fernan landscape. My hope is that this data is used by land managers to assess the magnitude of human influence on erosion processes throughout the watershed. My suggestion is that a sediment monitoring program be put into place to quantify sediment yields for the different sub-catchments throughout Fernan. Many of these smaller sub-basins are steep, and lack long-term sediment storage on a developed floodplain. Therefore, the baseline erosion rate can be converted to an annual sediment flux and used to directly compare to sediment yield from sediment monitoring in these regions. Steeper basins may have higher baseline rates of erosion based on the control of topography. Therefore, high modern sediment yields from these areas may be misinterpreted as a higher degree of human influence. Using the baseline rates I have provided, it is possible to separate the baseline erosion from modern sediment yield estimates. I believe that this will help to prioritize management efforts by sub-basin.

Controlling sediment erosion from land management is a first step towards addressing the causes of poor water quality in Fernan Lake, rather than just the symptoms.

REFERENCES

- Abbühl, L. M., Norton, K. P., Jansen, J. D., Schlunegger, F., Aldahan, A., & Possnert, G. (2011). Erosion rates and mechanisms of knickzone retreat inferred from ^{10}Be measured across strong climate gradients on the northern and central Andes Western Escarpment. *Earth Surface Processes and Landforms*, 36(11), 1464-1473.
- Aguilar, G., Carretier, S., Regard, V., Vassallo, R., Riquelme, R., & Martinod, J. (2014). Grain size-dependent ^{10}Be concentrations in alluvial stream sediment of the Huasco Valley, a semi-arid Andes region. *Quaternary Geochronology*, 19, 163-172.
- Ahnert, F. (1970). Functional relationships between denudation, relief, and uplift in large, mid-latitude drainage basins. *American Journal of Science*, 268(3), 243-263.
- Belmont, P., Pazzaglia, F. J., & Gosse, J. C. (2007). Cosmogenic ^{10}Be as a tracer for hillslope and channel sediment dynamics in the Clearwater River, western Washington State. *Earth and Planetary Science Letters*, 264(1), 123-135.
- Benito, G., & O'Connor, J. E. (2003). Number and size of last-glacial Missoula floods in the Columbia River valley between the Pasco Basin, Washington, and Portland, Oregon. *Geological Society of America Bulletin*, 115(5), 624-638.
- Bierman, P., & Steig, E. J. (1996). Estimating rates of denudation using cosmogenic isotope abundances in sediment. *Earth surface processes and landforms*, 21(2), 125-139.
- Binnie, S. A., Phillips, W. M., Summerfield, M. A., & Fifield, L. K. (2006). Sediment mixing and basin-wide cosmogenic nuclide analysis in rapidly eroding mountainous environments. *Quaternary Geochronology*, 1(1), 4-14.

- Binnie, S. A., Phillips, W. M., Summerfield, M. A., & Fifield, L. K. (2007). Tectonic uplift, threshold hillslopes, and denudation rates in a developing mountain range. *Geology*, 35(8), 743-746.
- Blaauw, M. (2010). Methods and code for 'classical' age-modelling of radiocarbon sequences. *quaternary geochronology*, 5(5), 512-518.
- Breckenridge, R. M., Othberg, K. L. (2004) Surficial geologic map of the Fernan Lake quadrangle, Kootenai County Idaho. 1:24,000. Idaho Geologic Survey.
[http://www.idahogeology.org/PDF/Digital_Data_\(D\)/Digital_Web_Maps_\(DWM\)/DWM-31-M.pdf](http://www.idahogeology.org/PDF/Digital_Data_(D)/Digital_Web_Maps_(DWM)/DWM-31-M.pdf) (01/01/2016)
- Brown, E. T., Stallard, R. F., Larsen, M. C., Raisbeck, G. M., & Yiou, F. (1995). Denudation rates determined from the accumulation of in situ-produced ^{10}Be in the Luquillo Experimental Forest, Puerto Rico. *Earth and Planetary Science Letters*, 129(1), 193-202.
- Brown, E. T., Stallard, R. F., Larsen, M. C., Bourlès, D. L., Raisbeck, G. M., & Yiou, F. (1998). Determination of predevelopment denudation rates of an agricultural watershed (Cayaguas River, Puerto Rico) using in-situ-produced ^{10}Be in river-borne quartz. *Earth and Planetary Science Letters*, 160(3), 723-728.
- Carretier, S., Regard, V., Vassallo, R., Martinod, J., Christophoul, F., Gayer, E., ... & Lagane, C. (2015). A note on ^{10}Be -derived mean erosion rates in catchments with heterogeneous lithology: examples from the western Central Andes. *Earth Surface Processes and Landforms*, 40(13), 1719-1729.

Chmeleff, J., von Blanckenburg, F., Kossert, K., & Jakob, D. (2010). Determination of the ^{10}Be half-life by multicollector ICP-MS and liquid scintillation counting. *Nuclear Instruments and Methods in Physics Research Section B: Beam Interactions with Materials and Atoms*, 268(2), 192-199.

Clague, J. J., Barendregt, R., Enkin, R. J., & Foit, F. F. (2003). Paleomagnetic and tephra evidence for tens of Missoula floods in southern Washington. *Geology*, 31(3), 247-250.

Codd, G. A., Bell, S. G., & Brooks, W. P. (1989). Cyanobacterial toxins in water. *Water Science and Technology*, 21(3), 1-13.

Codilean, A. T. (2006). Calculation of the cosmogenic nuclide production topographic shielding scaling factor for large areas using DEMs. *Earth Surface Processes and Landforms*, 31(6), 785-794.

Cyr, A. J., Granger, D. E., Olivetti, V., & Molin, P. (2014). Distinguishing between tectonic and lithologic controls on bedrock channel longitudinal profiles using cosmogenic ^{10}Be erosion rates and channel steepness index. *Geomorphology*, 209, 27-38.

DiBiase, R. A., Whipple, K. X., Heimsath, A. M., & Ouimet, W. B. (2010). Landscape form and millennial erosion rates in the San Gabriel Mountains, CA. *Earth and Planetary Science Letters*, 289(1), 134-144.

DiBiase, R. A., Heimsath, A. M., & Whipple, K. X. (2012). Hillslope response to tectonic forcing in threshold landscapes. *Earth Surface Processes and Landforms*, 37(8), 855-865.

Evans, K. V., Aleinikoff, J. N., Obradovich, J. D., & Fanning, C. M. (2000). SHRIMP U-Pb geochronology of volcanic rocks, Belt Supergroup, western Montana: evidence for

rapid deposition of sedimentary strata. *Canadian Journal of Earth Sciences*, 37(9), 1287-1300.

Fernan Lake Technical Advisory Committee. 2003. Draft Fernan Lake watershed management plan. Coeur d' Alene (ID).

Fillipone, J.A., and An Yin, 1994, Age and regional tectonic implications of Late Cretaceous thrusting and Eocene extension, Cabinet Mountains, northwest Montana and northern Idaho: *Geological Society of America Bulletin* v. 106, p. 1017-1032. in Lewis, R. S., Burmester, R. F., Breckenridge, R. M., McFaddan, M.D., Kauffman, J. D.. (2002) *Geologic map of the Coeur d'Alene 30x60 Quadrangle, Idaho. 1:100,000. Idaho Geologic Survey. 2002.*

Gilbert, G. K. (1877). *Report on the Geology of the Henry Mountains. US Government Printing Office.*

Goslar, T., Arnold, M., Bard, E., Kuc, T., Pazdur, M. F., Ralska-Jasiewiczowa, M., ... & Wieckowski, K. (1995). High concentration of atmospheric ¹⁴C during the Younger Dryas cold episode. *Nature*, 377(6548), 414-417.

Gosse, J. C., & Phillips, F. M. (2001). Terrestrial in situ cosmogenic nuclides: theory and application. *Quaternary Science Reviews*, 20(14), 1475-1560.

Granger, D. E., Kirchner, J. W., & Finkel, R. (1996). Spatially averaged long-term erosion rates measured from in situ-produced cosmogenic nuclides in alluvial sediment. *The Journal of Geology*, 249-257.

Hack, J. T. (1973). Stream-profile analysis and stream-gradient index. *Journal of Research of the US Geological Survey*, 1(4), 421-429.

- Hallett, D. J., Hills, L. V., & Clague, J. J. (1997). New accelerator mass spectrometry radiocarbon ages for the Mazama tephra layer from Kootenay National Park, British Columbia, Canada. *Canadian Journal of Earth Sciences*, 34(9), 1202-1209.
- Hanson, M. A., Lian, O. B., & Clague, J. J. (2012). The sequence and timing of large late Pleistocene floods from glacial Lake Missoula. *Quaternary Science Reviews*, 31, 67-81.
- Harrison, J. E., & Grimes, D. J. (1970). Mineralogy and geochemistry of some Belt rocks, Montana and Idaho. US Government Printing Office.
- Hidy, Alan. "Cosmogenic Nuclide Quantification of Paleo-fluvial Sedimentation Rates in Response to Climate Change." PhD diss., 2013.
- Higuera, P. (2008). MCAgeDepth 0.1: Probabilistic age-depth models for continuous sediment records. Montana State University. Available at: <http://www.montana.edu/phiguera>.
- Higuera, P. E., Brubaker, L. B., Anderson, P. M., Hu, F. S., & Brown, T. A. (2009). Vegetation mediated the impacts of postglacial climate change on fire regimes in the south-central Brooks Range, Alaska. *Ecological Monographs*, 79(2), 201-219.
- Hippe, K., Kober, F., Zeilinger, G., Ivy-Ochs, S., Maden, C., Wacker, L., ... & Wieler, R. (2012). Quantifying denudation rates and sediment storage on the eastern Altiplano, Bolivia, using cosmogenic ^{10}Be , ^{26}Al , and in situ ^{14}C . *Geomorphology*, 179, 58-70.
- Idaho Department of Environmental Quality, Boise, Idaho. (2011). Idaho's 2010 integrated report.

- Idaho Department of Environmental Quality, Coeur d'Alene Regional Office. (2013). Coeur d'Alene Lake and River subbasin assessment and total maximum daily loads: 2013 Fernan Lake Addendum.
- Insel, N., Ehlers, T. A., Schaller, M., Barnes, J. B., Tawackoli, S., & Poulsen, C. J. (2010). Spatial and temporal variability in denudation across the Bolivian Andes from multiple geochronometers. *Geomorphology*, 122(1), 65-77.
- James, C. S. (1985). Sediment transfer to overbank sections. *Journal of Hydraulic Research*, 23(5), 435-452.
- Judson, S., & Ritter, D. F. (1964). Rates of regional denudation in the United States. *Journal of Geophysical Research*, 69(16), 3395-3401.
- Karwan, D. L., Gravelle, J. A., & Hubbart, J. A. (2007). Effects of timber harvest on suspended sediment loads in Mica Creek, Idaho. *Forest Science*, 53(2), 181-188.
- Kirchner, J. W., Finkel, R. C., Riebe, C. S., Granger, D. E., Clayton, J. L., King, J. G., & Megahan, W. F. (2001). Mountain erosion over 10 yr, 10 ky, and 10 my time scales. *Geology*, 29(7), 591-594.
- Kohl, C. P., & Nishiizumi, K. (1992). Chemical isolation of quartz for measurement of in-situ-produced cosmogenic nuclides. *Geochimica et Cosmochimica Acta*, 56(9), 3583-3587.
- LaCroix, T. (2015) A nutrient mass balance of Fernan Lake, Idaho and directions for future research (Master's Thesis). Retrieved from University of Idaho, ProQuest Dissertations Publishing, 2015 (no. 1605419)
- Lal, D. (1991). Cosmic ray labeling of erosion surfaces: in situ nuclide production rates and erosion models. *Earth and Planetary Science Letters*, 104(2-4), 424-439.

- Li, Y. K. (2013). Determining topographic shielding from digital elevation models for cosmogenic nuclide analysis: a GIS approach and field validation. *Journal of Mountain Science*, 10(3), 355-362.
- Matmon, A., Bierman, P. R., Larsen, J., Southworth, S., Pavich, M., Finkel, R., & Caffee, M. (2003). Erosion of an ancient mountain range, the Great Smoky Mountains, North Carolina and Tennessee. *American Journal of Science*, 303(9), 817-855.
- Megahan, W. F., King, J. G., & Seyedbagheri, K. A. (1995). Hydrologic and erosional responses of a granitic watershed to helicopter logging and broadcast burning. *Forest Science*, 41(4), 777-795.
- Menard, H. W. (1961). Some rates of regional erosion. *The Journal of Geology*, 154-161.
- Montgomery, D. R., Buffington, J. M., Peterson, N. P., Schuett-Hames, D., & Quinn, T. P. (1996). Stream-bed scour, egg burial depths, and the influence of salmonid spawning on bed surface mobility and embryo survival. *Canadian Journal of Fisheries and Aquatic Sciences*, 53(5), 1061-1070.
- Mueller, E. R., & Pitlick, J. (2013). Sediment supply and channel morphology in mountain river systems: 1. Relative importance of lithology, topography, and climate. *Journal of Geophysical Research: Earth Surface*, 118(4), 2325-2342.
- Norton, K. P., von Blanckenburg, F., DiBiase, R., Schlunegger, F., & Kubik, P. W. (2011). Cosmogenic ^{10}Be -derived denudation rates of the Eastern and Southern European Alps. *International Journal of Earth Sciences*, 100(5), 1163-1179.

O'Connor, J. E. (2009, October). Late Pleistocene Missoula Floods—15,000-20,000 Calendar Years Before Present From Radiocarbon Dating. In 2009 Portland GSA Annual Meeting.

Othberg, K. L., & Breckenridge, R. M. (1998). Paleogeomorphic evolution of the Columbia River basalt embayments, western margin of the Northern Rocky Mountains: Part

I. Basalt stratigraphy and tectonics in the Coeur d'Alene area: Geological Society of America Abstracts with Programs, 30(6), 33. In Breckenridge, R. M., Othberg, K. L.

(2004) Surficial geologic map of the Fernan Lake quadrangle, Kootenai County Idaho. 1:24,000. Idaho Geologic Survey.

[http://www.idahogeology.org/PDF/Digital_Data_\(D\)/Digital_Web_Maps_\(DWM\)/DW-M-31-M.pdf](http://www.idahogeology.org/PDF/Digital_Data_(D)/Digital_Web_Maps_(DWM)/DW-M-31-M.pdf) (01/01/2016)

Palumbo, L., Hetzel, R., Tao, M., & Li, X. (2010). Topographic and lithologic control on catchment-wide denudation rates derived from cosmogenic ^{10}Be in two mountain ranges at the margin of NE Tibet. *Geomorphology*, 117(1), 130-142.

Phillips, J. (2003). Alluvial storage and the long-term stability of sediment yields. *Basin Research*, 15(2), 153-163.

Puchol, N., Lavé, J., Lupker, M., Blard, P. H., Gallo, F., France-Lanord, C., & ASTER Team.

(2014). Grain-size dependent concentration of cosmogenic ^{10}Be and erosion dynamics in a landslide-dominated Himalayan watershed. *Geomorphology*, 224, 55-68.

Ramsey, C. B. (2008). Deposition models for chronological records. *Quaternary Science Reviews*, 27(1), 42-60.

- Ramsey, C. B. (2009). Bayesian analysis of radiocarbon dates. *Radiocarbon*, 51(1), 337-360.
- Reimer, P. J., Bard, E., Bayliss, A., Beck, J. W., Blackwell, P. G., Ramsey, C. B., ... & Grootes, P. M. (2013). Selection and treatment of data for radiocarbon calibration: an update to the International Calibration (IntCal) criteria. *Radiocarbon*, 55(4), 1923-1945.
- Reneau, S. L., & Dietrich, W. E. (1991). Erosion rates in the southern Oregon Coast Range: Evidence for an equilibrium between hillslope erosion and sediment yield. *Earth Surface Processes and Landforms*, 16(4), 307-322.
- Rhodes, B. P., & Hyndman, D. W. (1984). Kinematics of mylonites in the Priest River" metamorphic core complex," northern Idaho and northeastern Washington. *Canadian Journal of Earth Sciences*, 21(10), 1161-1170.
- Riebe, C. S., Kirchner, J. W., Granger, D. E., & Finkel, R. C. (2000). Erosional equilibrium and disequilibrium in the Sierra Nevada, inferred from cosmogenic ^{26}Al and ^{10}Be in alluvial sediment. *Geology*, 28(9), 803-806.
- Roberts, R. G., & Church, M. (1986). The sediment budget in severely disturbed watersheds, Queen Charlotte Ranges, British Columbia. *Canadian Journal of Forest Research*, 16(5), 1092-1106.
- Roering, J. J., Kirchner, J. W., & Dietrich, W. E. (1999). Evidence for nonlinear, diffusive sediment transport on hillslopes and implications for landscape morphology. *Water Resources Research*, 35(3), 853-870.
- Safran, E. B., Bierman, P. R., Aalto, R., Dunne, T., Whipple, K. X., & Caffee, M. (2005). Erosion rates driven by channel network incision in the Bolivian Andes. *Earth Surface Processes and Landforms*, 30(8), 1007-1024.

- Schildgen, T. F., Phillips, W. M., & Purves, R. S. (2005). Simulation of snow shielding corrections for cosmogenic nuclide surface exposure studies. *Geomorphology*, 64(1), 67-85.
- Schumm, S. A. (1963). The disparity between present rates of denudation and orogeny. US Government Printing Office.
- Siregar, A., Kleber, M., Mikutta, R., & Jahn, R. (2005). Sodium hypochlorite oxidation reduces soil organic matter concentrations without affecting inorganic soil constituents. *European Journal of Soil Science*, 56(4), 481-490.
- Stone, J. O. (2000). Air pressure and cosmogenic isotope production. *Journal of Geophysical Research: Solid Earth*, 105(B10), 23753-23759.
- Stuiver, M., Reimer, P. J., & Reimer, R. W. (2005). CALIB 7.1.
- Trimble, S. W. (1977). The fallacy of stream equilibrium in contemporary denudation studies. *American Journal of Science*, 277(7), 876-887.
- Trimble, S. W. (1983). A sediment budget for Coon Creek basin in the Driftless Area, Wisconsin, 1853-1977. *American Journal of Science*, 283(5), 454-474.
- Trimble, S. W. (1999). Decreased rates of alluvial sediment storage in the Coon Creek Basin, Wisconsin, 1975-93. *Science*, 285(5431), 1244-1246.
- Von Blanckenburg, F. (2005). The control mechanisms of erosion and weathering at basin scale from cosmogenic nuclides in river sediment. *Earth and Planetary Science Letters*, 237(3), 462-479.
- Walling, D. E., & He, Q. (1998). The spatial variability of overbank sedimentation on river floodplains. *Geomorphology*, 24(2), 209-223.

- Walling, D. E. (1999). Linking land use, erosion and sediment yields in river basins. *Hydrobiologia*, 410, 223-240.
- Yang, D., Kanae, S., Oki, T., Koike, T., & Musiake, K. (2003). Global potential soil erosion with reference to land use and climate changes. *Hydrological processes*, 17(14), 2913-2928.
- Yanites, B. J., Tucker, G. E., & Anderson, R. S. (2009). Numerical and analytical models of cosmogenic radionuclide dynamics in landslide-dominated drainage basins. *Journal of Geophysical Research: Earth Surface*, 114(F1).
- Zweck, C., Zreda, M., & Desilets, D. (2013). Snow shielding factors for cosmogenic nuclide dating inferred from Monte Carlo neutron transport simulations. *Earth and Planetary Science Letters*, 379, 64-71.

FIGURES

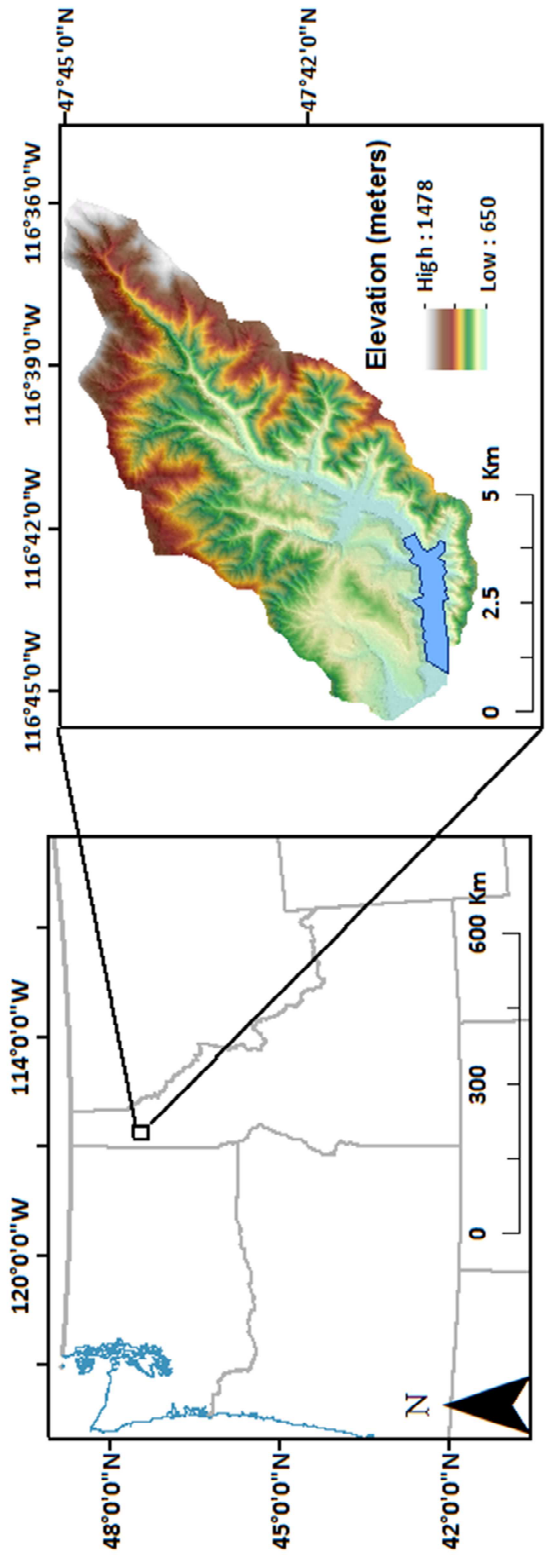


Figure 1: The Fernan watershed is located in the Panhandle of northern Idaho, just east of Coeur d'Alene in Kootenai County.

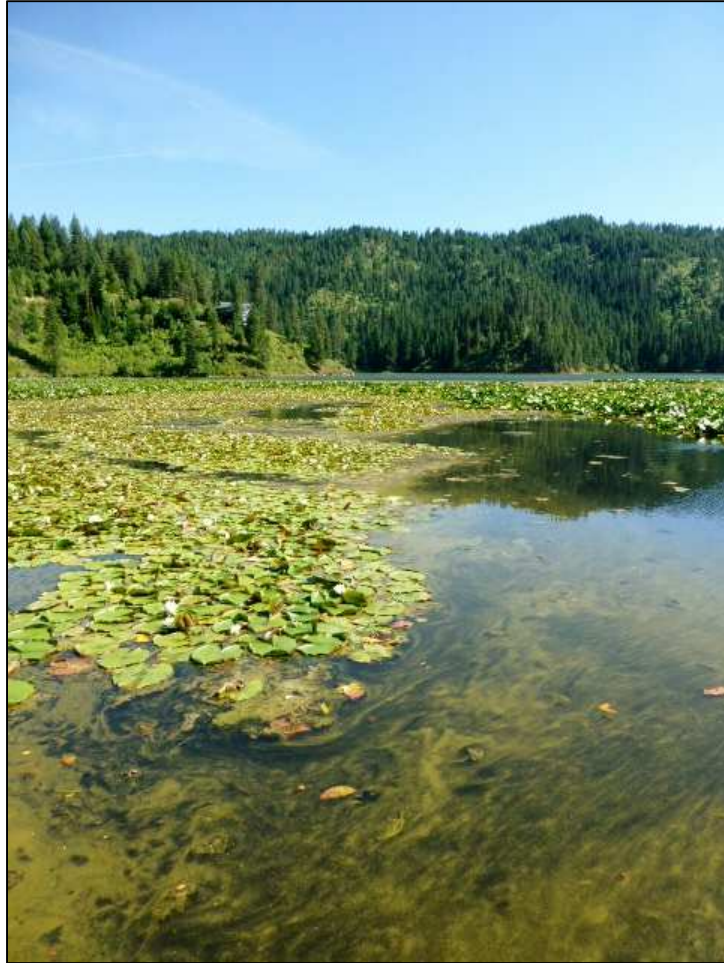


Figure 2: Blue-green algae in Fernan Lake. Some species found among these blooms are capable of producing toxins harmful to both humans and pets. Photo taken from the MILES program (Managing Idaho's Landscapes for Ecosystem Services) website: idahoecosystems-pre.nkn.uidaho.edu

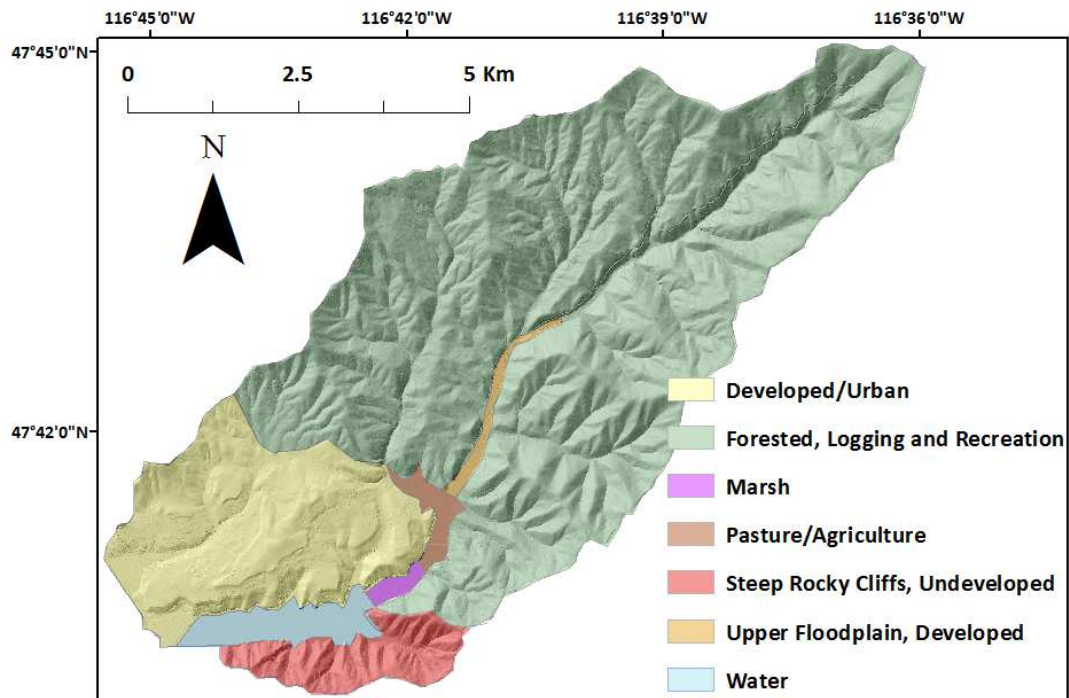


Figure 3: A map of land use throughout the Fernan watershed



Figure 4: Road material from the Fernan Creek Road Project stored along the middle reach of Fernan Creek. Photo taken from IDEQ (2013).

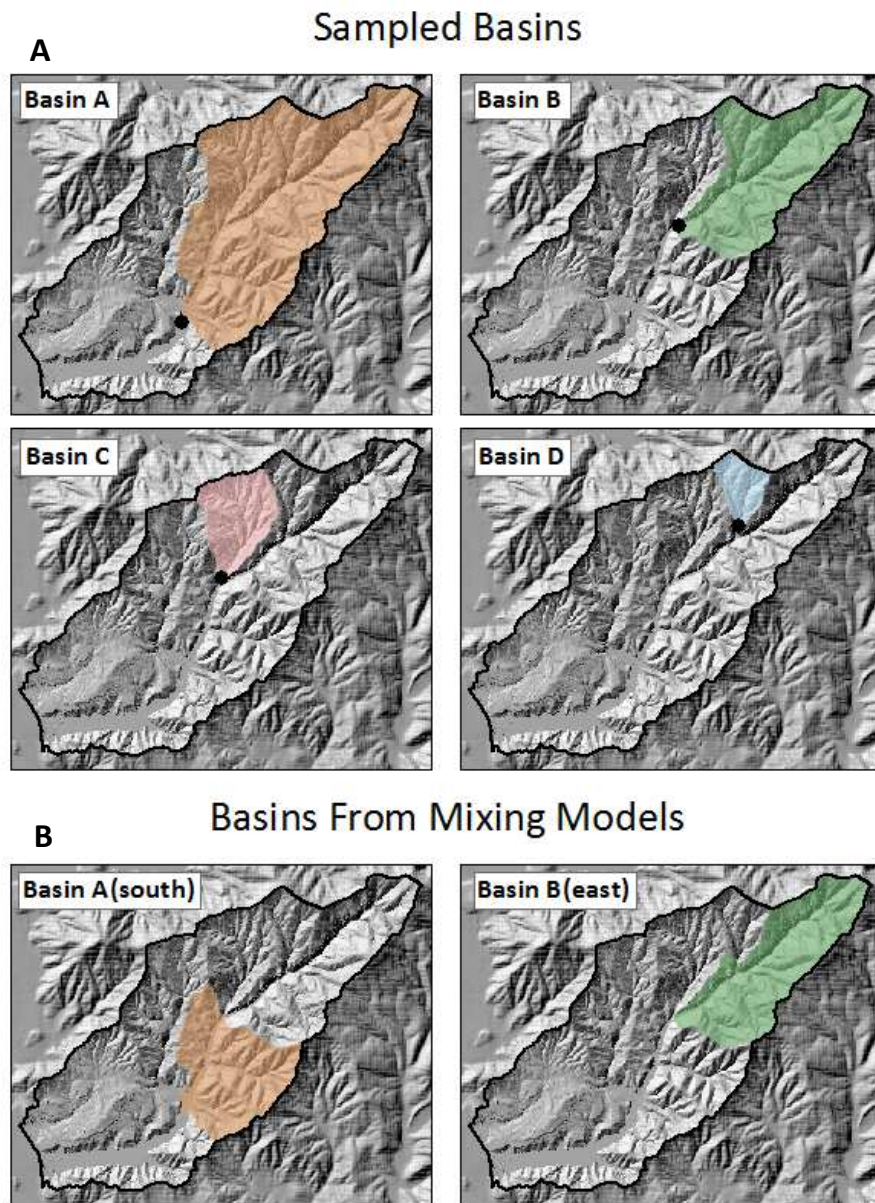


Figure 5: Fernan basins where erosion is inferred from measured concentrations of ^{10}Be [A] and from sediment mixing models [B]. Erosion for Basin A(south) is determined by subtracting the sediment flux of basins B and C from that of A and dividing by the area of Basin A(south). B(east) is similarly found using basins C and D.

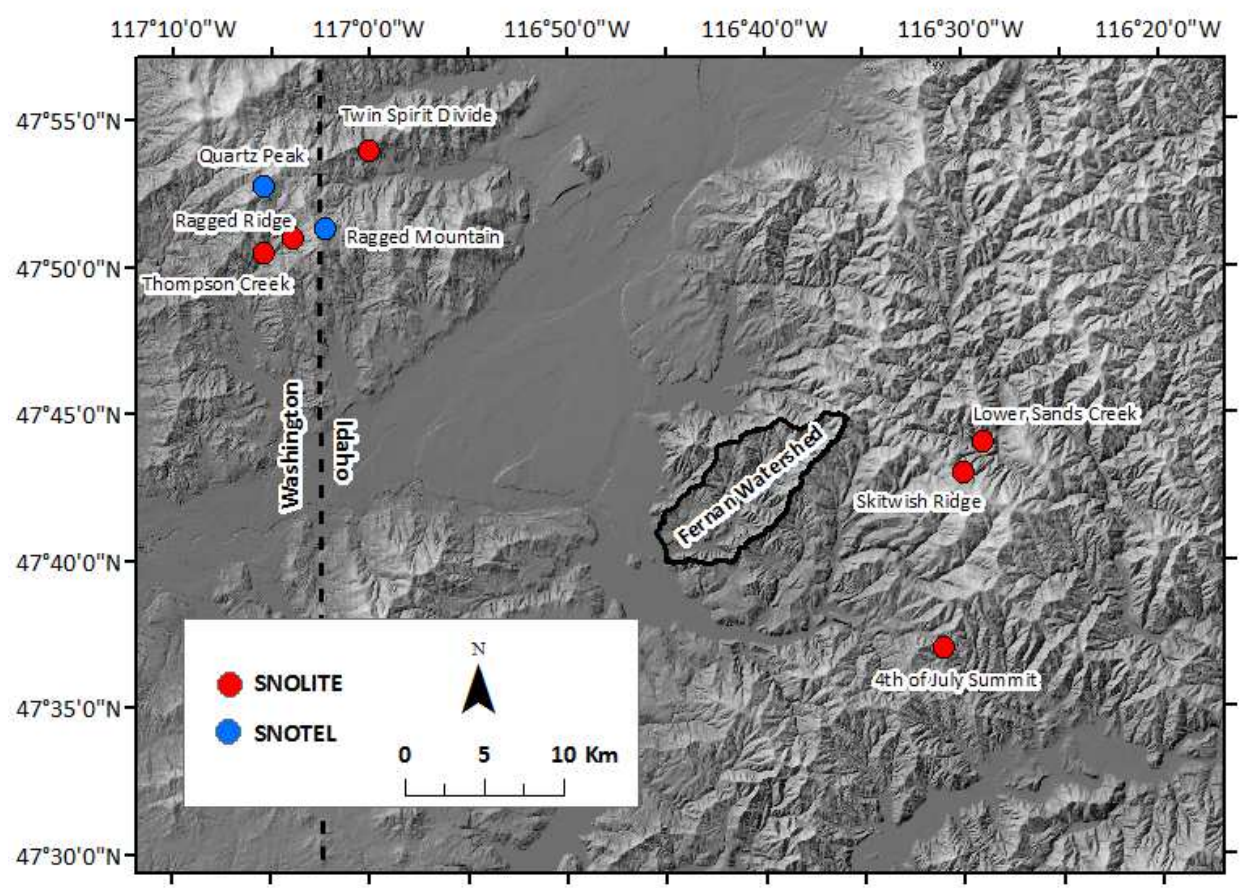


Figure 6: Locations of NRCS SNOTEL and SNOLITE sites used for calculating snow-shielding corrections. These sites all fall within one-third of a degree latitude and their elevations approximate the elevation range of the Fernan Watershed. 30-year median snow depth and snow-water equivalent data was downloaded from: <http://www.wcc.nrcs.usda.gov/snow/>

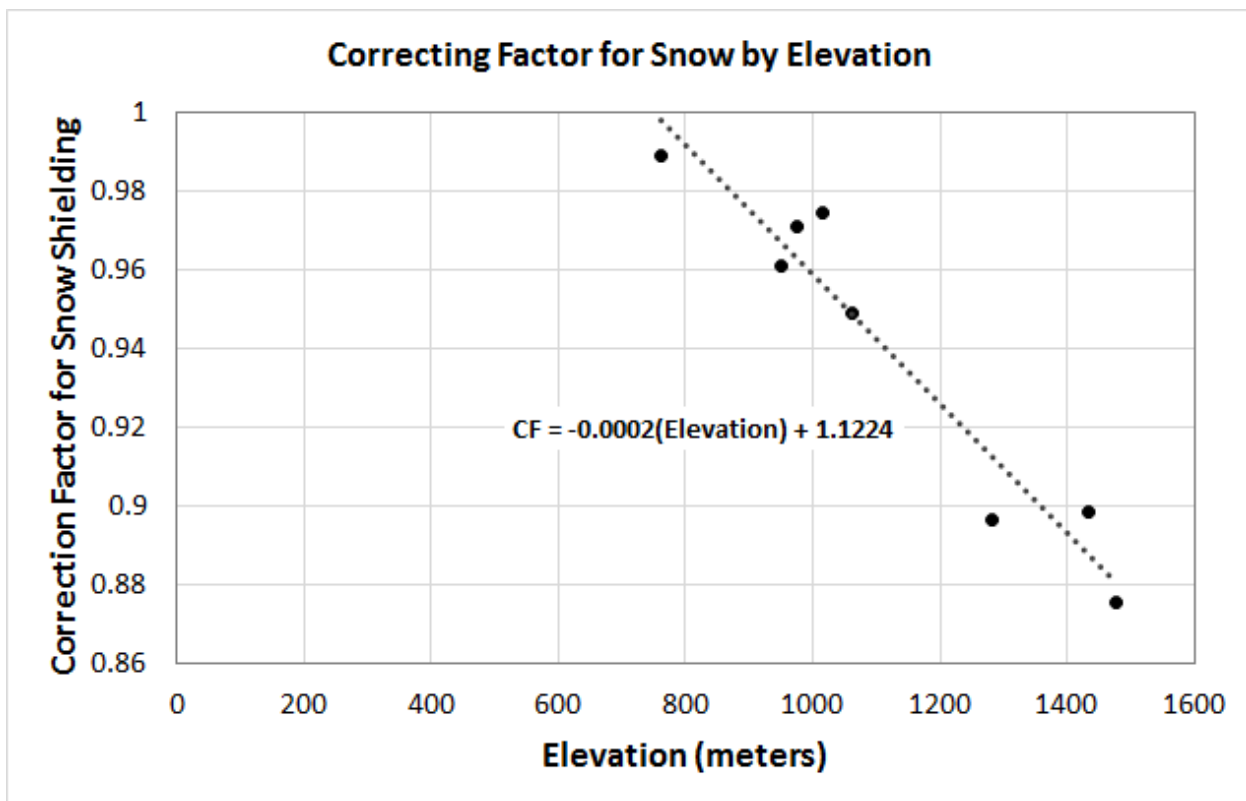


Figure 7: The modeled relationship for snow CF by elevation. The relationship was modeled from data collected from nearby SNOTEL and SNOLITE sites and used to determine basin-average shielding coefficients.

Correction Factor for Snow Shielding

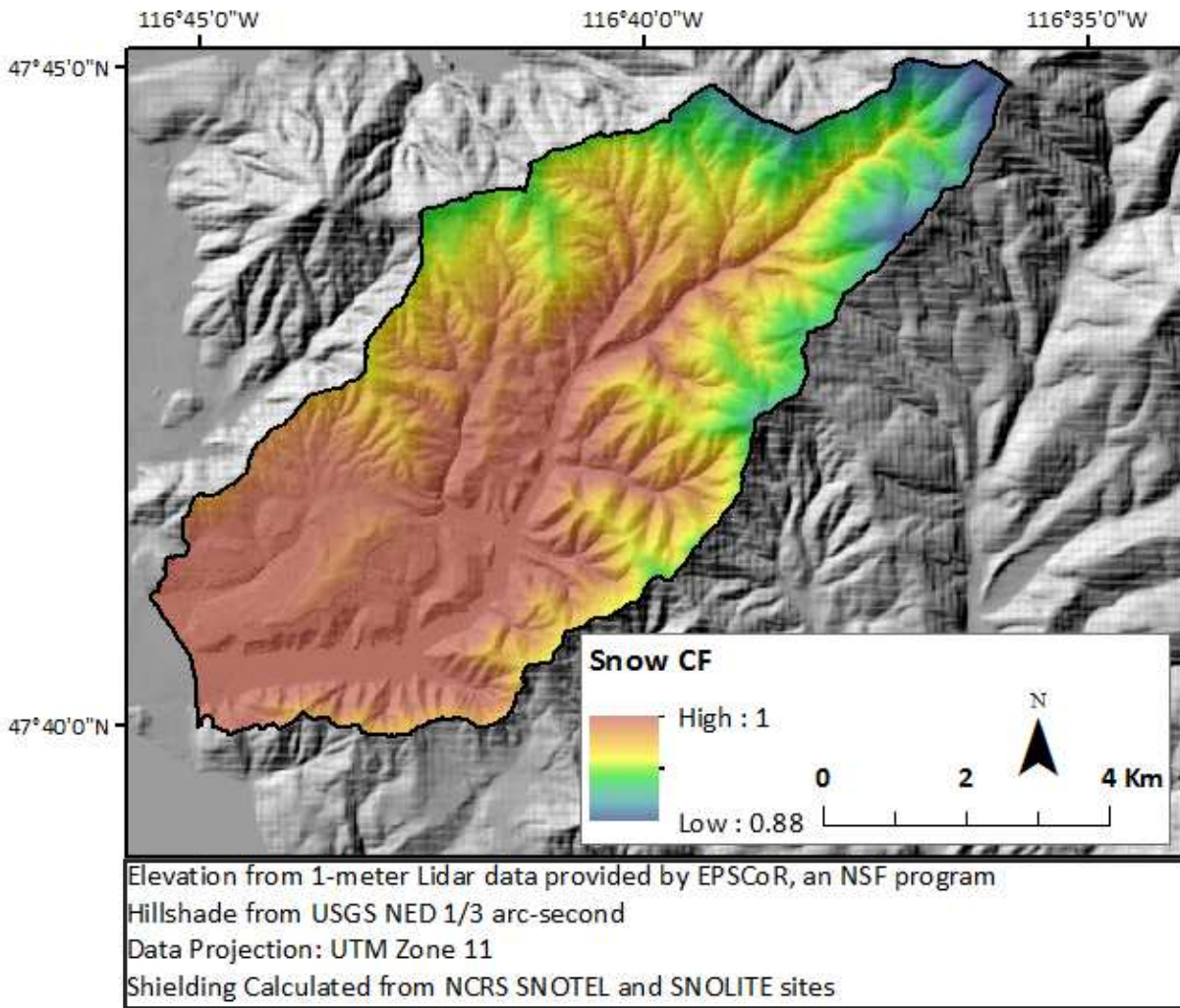


Figure 8: A map of snow shielding (CF) throughout the Fernan watershed. The correction factor is the fraction of surface production effective at the soil surface. Therefore, cold colors (blue and green) indicate a higher degree of shielding.

Correction Factor for Topographic Shielding

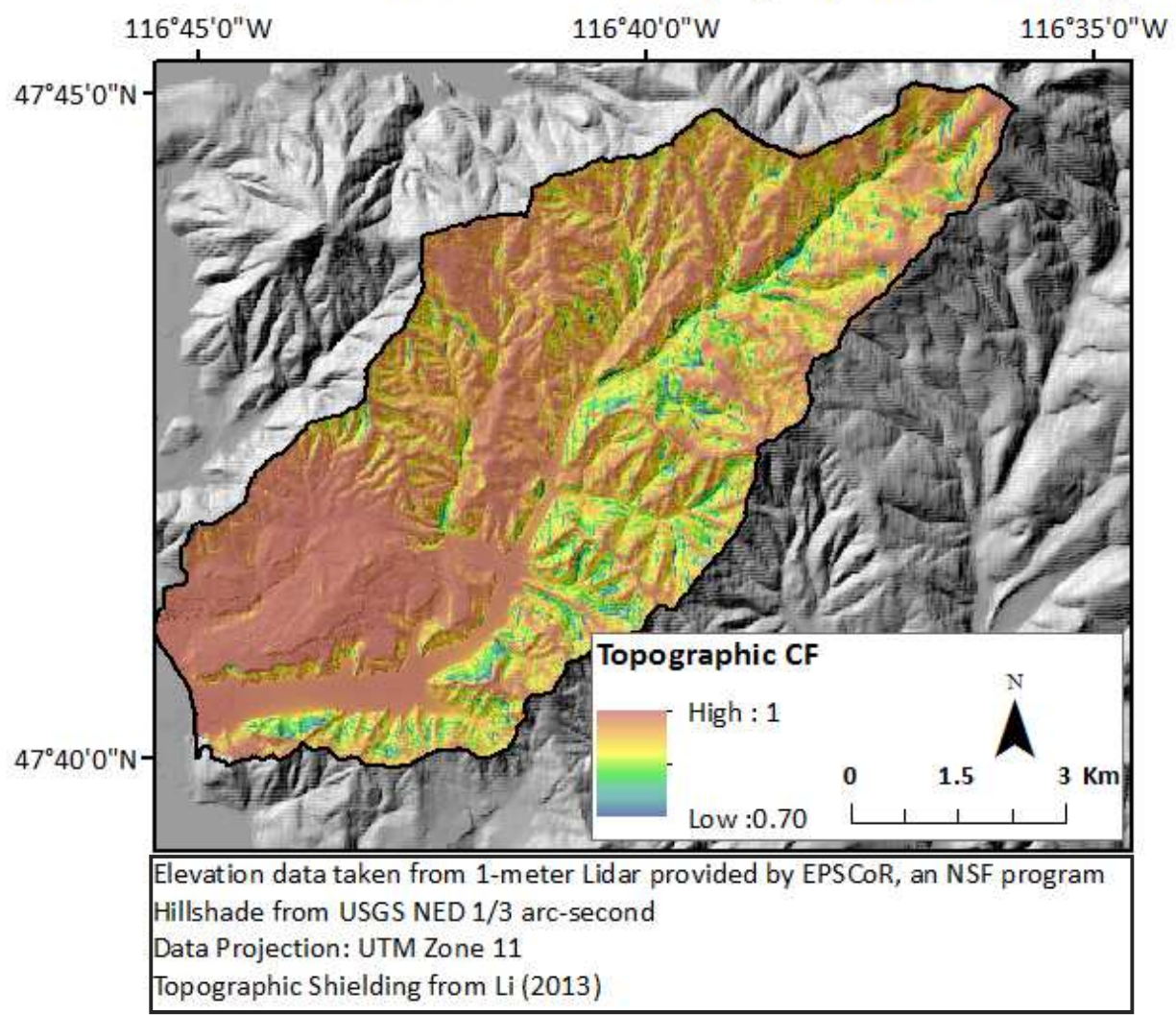


Figure 9: Correction factor for topographic shielding. Shielding is calculated using the hillshading approach by Codilean (2006) from the ArcGIS toolbox by Li (2013).



Figure 10: The Geoprobe coring device used to extract sediment cores from the floodplain.

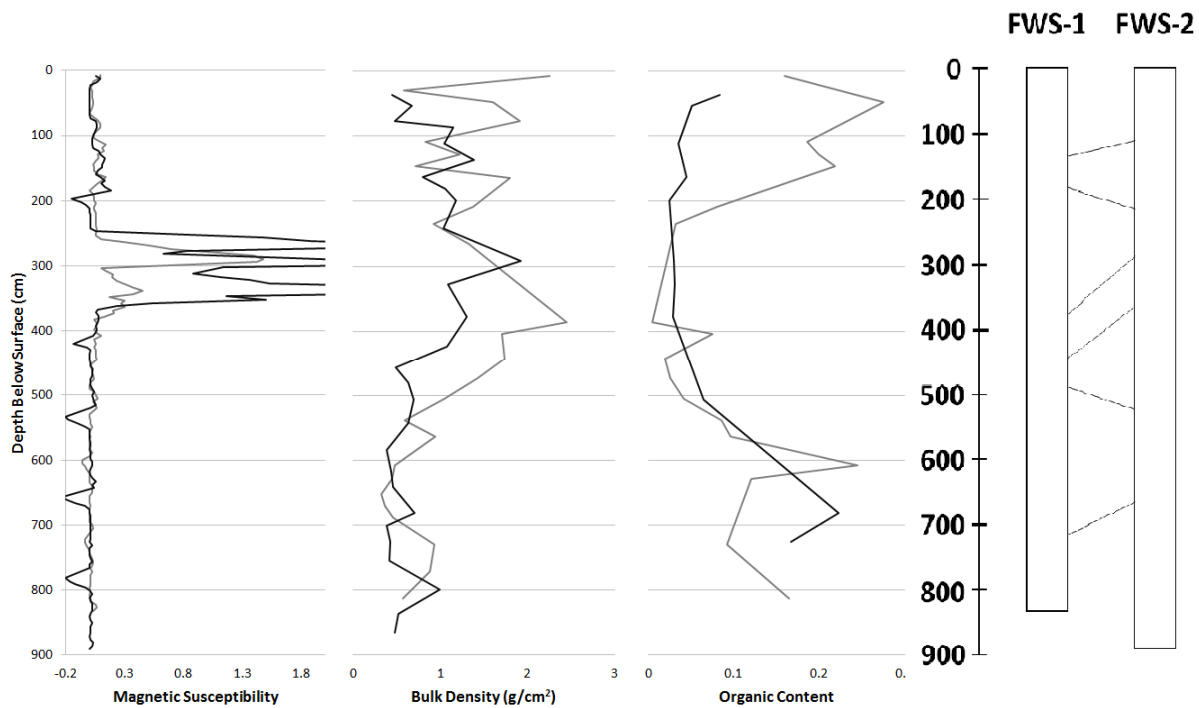


Figure 11: Graphs of the change in magnetic susceptibility, bulk density, and organic content with depth. These properties were used to correlate depths between cores (left).

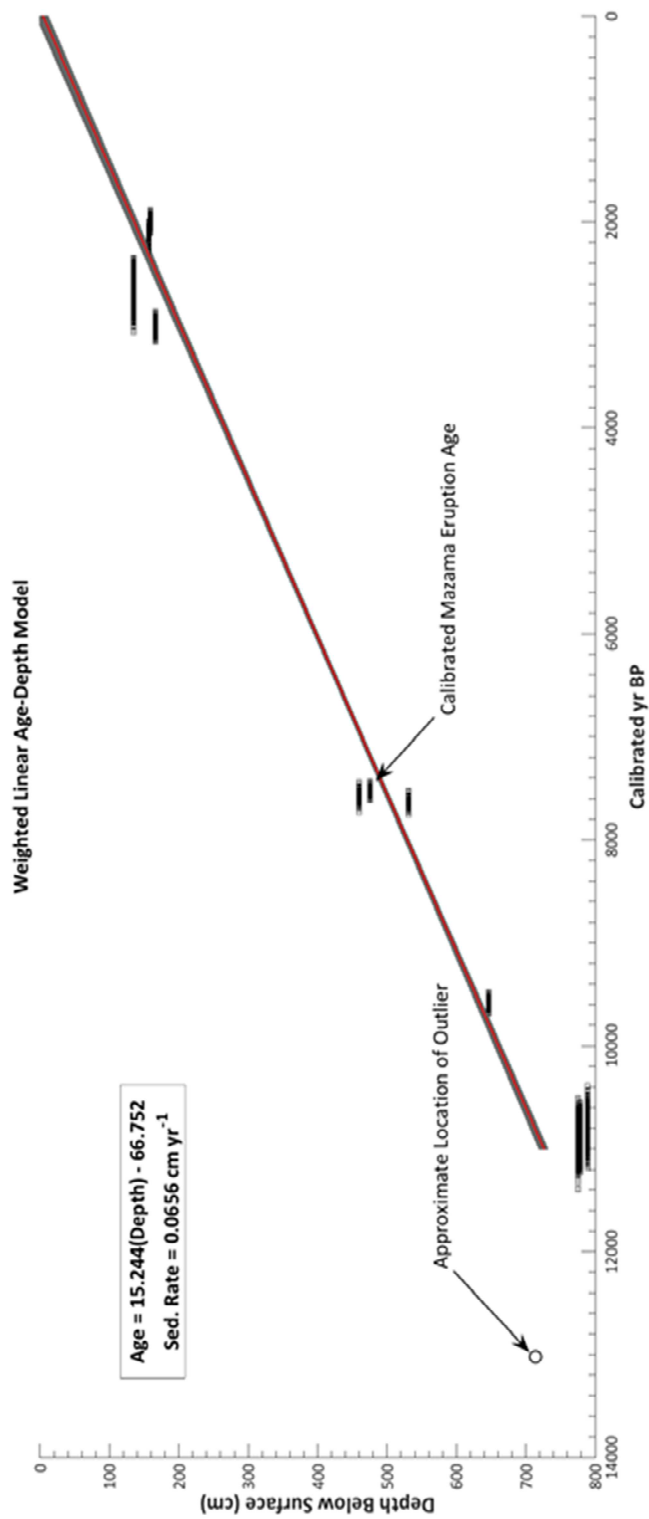


Figure 12: Age-Depth model of deposited layers in sediment cores. The model is produced using a Monte-Carlo simulation of calibrated ages for each sample. Each linear model is based on weighted linear-regression, weighting each sample by the inverse of its standard deviation.

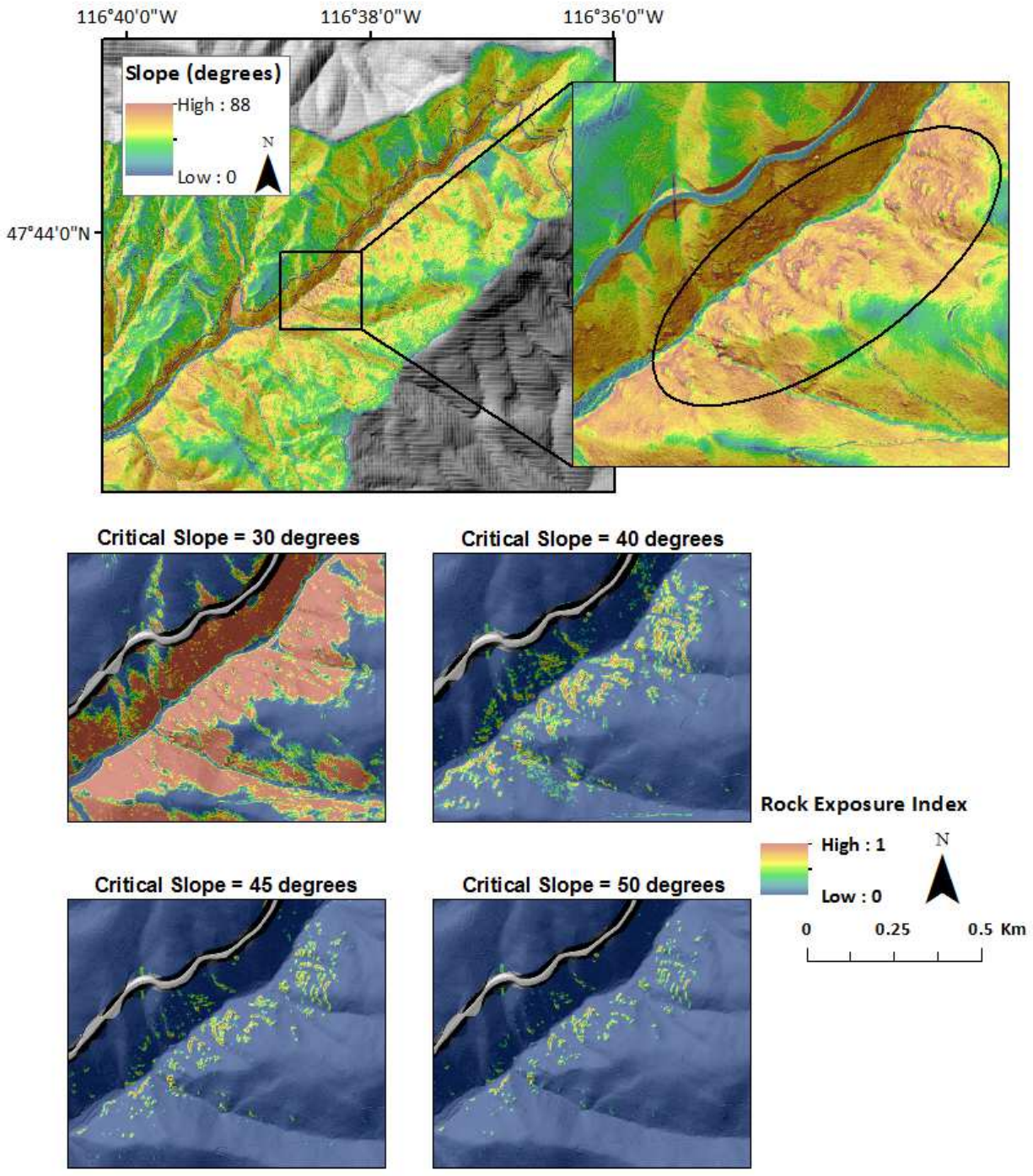


Figure 13: Top: Outcrops apparent from Lidar-derived slope overlaying a hillshade layer. Bottom: Outcropping predicted by the rock exposure index with increasing values for critical slope.

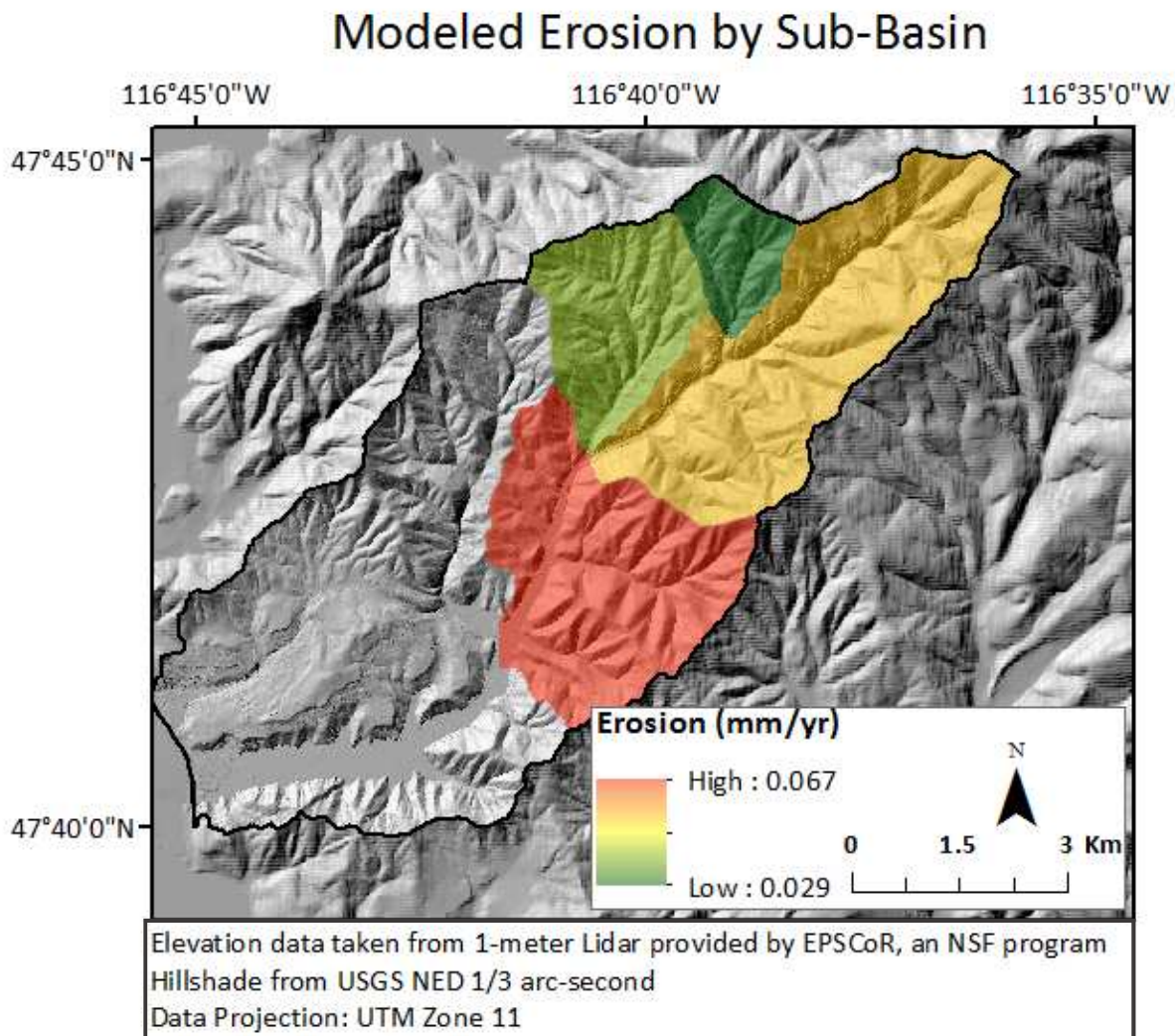


Figure 14: The distribution of erosion rates throughout the watershed. Erosion appears to increase moving from the headwaters downstream toward the lake.

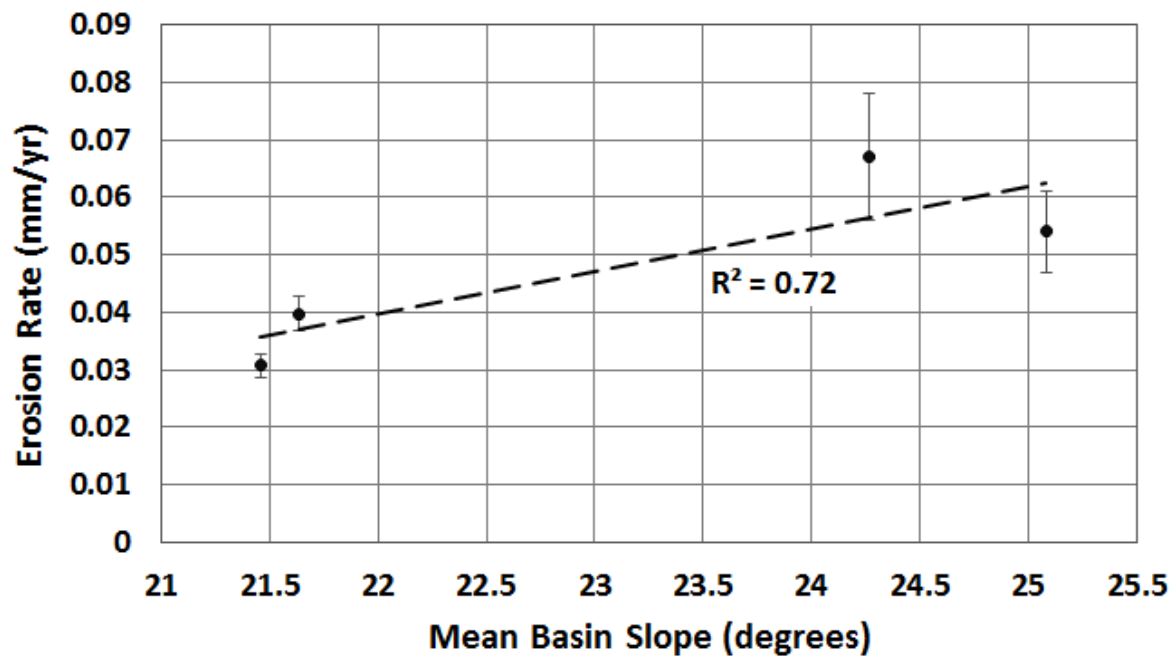


Figure 15: The modeled relationship between mean basin slope and erosion rate.

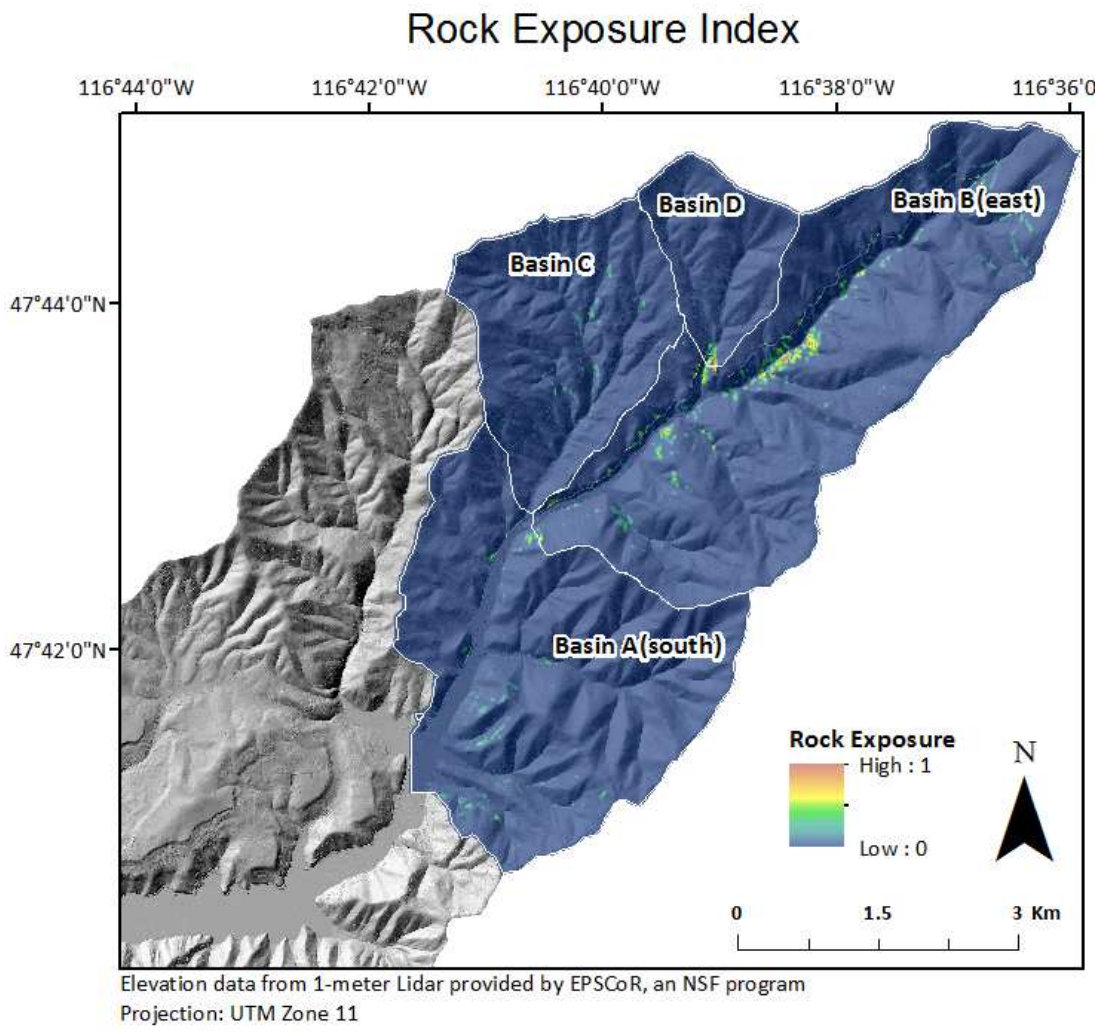


Figure 16: Outcrops predicted by the rock exposure index using a critical slope value of 45 degrees. REI data has been recalculated using "Focal Statistics" for a circle with a radius of 20 for display purposes.

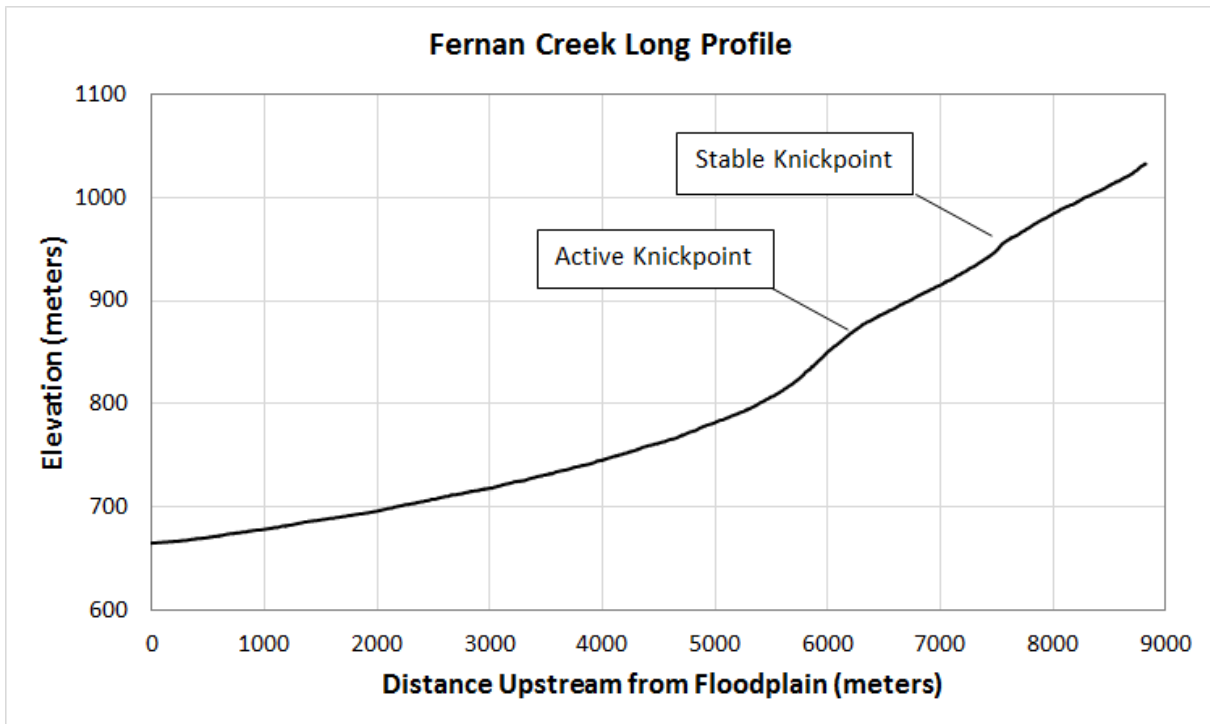


Figure 17: The long-profile of Fernan Creek from the floodplain upstream taken from 1-meter Lidar. The knickpoint from 800-900m appears to be actively incising, whereas the knickpoint further upstream is smaller and appears to be the result of contrasting erodibility across lithologic formations.

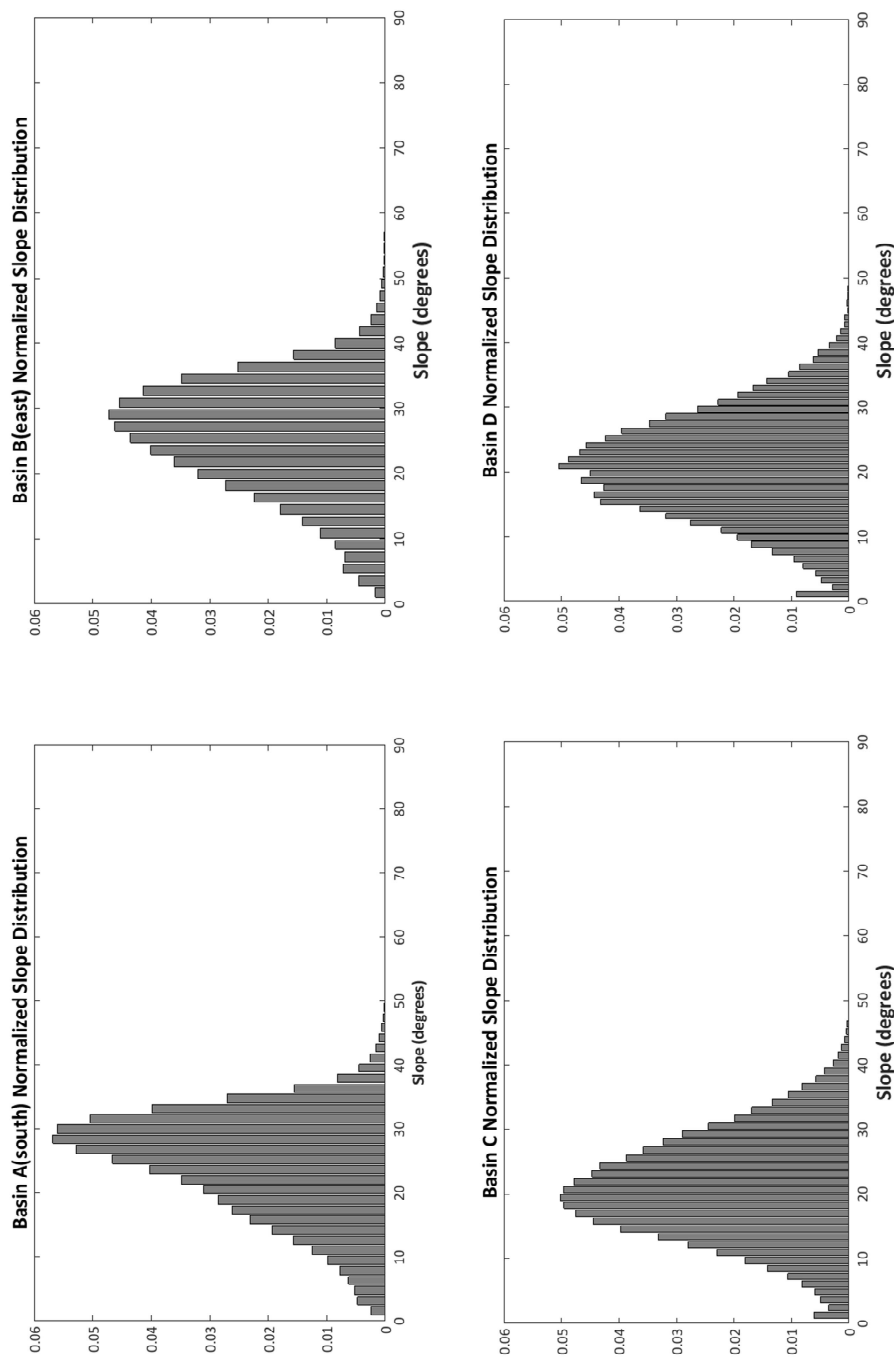


Figure 18: Distribution of slopes by basin. B(east), C, and D exhibit approximately normal distributions, and B(east) has a small fraction of higher slope values. Basin A slopes are heavily distributed around 25-30 degrees and fall off sharply beyond 30.

TABLES

TABLE 1: EROSION RATES FROM ^{10}Be CONCENTRATIONS (RAW DATA)

Basin	Concentration (Atoms ^{10}Be /g SiO $_2$)	Standard Deviation	Relative Uncertainty	Production Rate	Raw Erosion (mm/year)	Residence Time
A(sand)	135,000	3,484	2.6%	12.2	0.054	11,000
B(sand)	157,000	5,259	3.3%	13.2	0.050	12,000
C(sand)	178,000	4,333	2.4%	11.8	0.040	15,000
D(sand)	264,000	5,338	2.0%	13.5	0.031	20,000
A(gravel)	102,000	3,772	3.7%	12.2	0.072	8,500
C(gravel)	175,000	4,332	2.5%	11.8	0.040	14,000
D(gravel)	156,000	6,193	4.0%	13.5	0.052	11,500

TABLE 2: EROSION MODELING CORRECTIONS:

Basin	Raw Production Hidy (2013)	CF Snow	CF Topography	Production Rate All Corrections
A	12.2	.964	.964	11.7
B	13.2	.949	.963	12.4
C	11.8	.970	.971	11.1
D	13.5	.943	.972	12.4

Corrections of surface production rates for each sub-basin. Surface production units are in atoms $\text{g}^{-1} \text{yr}^{-1}$. CF factors are multiplied by raw or quartz-corrected production rates to account for shielding of cosmic rays by snow or topography.

TABLE 3: SNOW-WATER EQUIVALENT DATA

Site	Elevation (m)	January	February	March	April	May	Annual Average
Thompson Creek	762	0	10.7	10.7	0	0	1.8
Lower Sands	961	0	0	41.1	42.9	34.0	9.8
4 th of July	957	7.6	19.0	21.6	8.6	0	4.7
Ragged Ridge	1016	9.4	17.5	30.1	2.5	0	4.1
Twin Spirit	1061	15.7	24.9	30.2	30.0	0	8.4
Ragged Mountain	1280	24.9	40.1	71.9	4.70	9.4	17.5
Skitwish	1478	0	0	63.5	72.6	54.9	21.2

Snow-water equivalent monthly 30-year median data (in cm) used to calculate snow correction factors.

*TABLE 4: B(EAST) MIXING MODEL
(SNOW-CORRECTED VALUES)*

Basin	Erosion (mm/year)	Area (m ²)	Sed. Flux (m ³ /year)
B	0.048	147,94,500	710
D	0.029	22,33,680	65
B(east)	0.051	12,560,820	645

*TABLE 5: A(SOUTH) MIXING MODEL
(SNOW-CORRECTED VALUES)*

Basin	Erosion (mm/year)	Area (m ²)	Sed. Flux (m ³ /year)
A	0.052	295,43,170	1570
B	0.048	14,794,500	710
C	0.039	5,165,200	210
A(south)	0.066	100,95,650	1100

TABLE 6: ¹⁴C AGES OF SAMPLES

Sample	Sample Type	Depth (cm)	¹⁴ C Age	¹⁴ C Error	Calibrated yr BP 95% confidence	
					Upper	Lower
1	Charcoal	135	2,605	78	-927	-486
2	Charcoal	157	2,139	22	-351	-91
3	Charcoal	159	2,018	22	-56	52
4	Charcoal	166	2,876	22	-1123	-977
5	Charcoal	381	6,661	26	-5632	-5541
6	Woody Plant	475	6,780	35	-5726	-5631
7	Woody Plant	531	8,603	33	-7709	-7573
8	Plant	646	13,011	60	-13848	-13360
9	Seed	775	9,621	90	-9255	-8765
10	Seed	778	9,572	67	-9211	-8761
11	Seed	789	9,464	59	-9125	-8613

TABLE 7: TOPOGRAPHY BY SUB-BASIN

Basin	Mean Slope (degrees)	Slope Std. Dev.	Max. Relief (m)	Mean Relief (m)	Area (m ²)	REI (%)
A	23.7	8.3	825	315	29,543,171	0.26
B	24.2	8.5	782	366	14,794,499	0.36
C	21.7	7.4	508	235	5,165,200	0.15
D	21.3	7.1	484	274	2,233,678	0.12
A(south)	24.0	8.1	563	183	10,095,650	0.18
B(east)	24.7	8.7	782	363	12,560,821	0.41

Appendix 1: Photos of core segments



Core 2, Segment 1: Length-93 cm, mostly silts/clays



Core 2, Segment 2: Length-94 cm, mostly silts and clays, bands of charcoal from 80-90 cm on tape



Core 2, Segment 3: Length- 118 cm, all Mazama ash



Core 2, Segment 4: Length- 105 cm, top is Mazama ash, minor charcoal from 50-90 cm on tape



Core 2, Segment 5: Length- 113 cm, mainly silts/clays, minor plant material and charcoal throughout



Core 2, Segment 6: Length- 121 cm dark brow to black silts and clays



Core 2, Segment 7: Length- 121 cm, dark brown to black silts and clays, seed pods present

Diatom layers present in segments: 1, 4, 5, and 8